ENSO and internal sea surface temperature variability in the tropical Indian Ocean since 1675

Maike Leupold[1], Miriam Pfeiffer[2], Takaaki K. Watanabe[3], Lars Reuning[2], Dieter Garbe-Schönberg[2], Chuan-Chou Shen[4,5,6], Geert-Jan A. Brummer[7]

[1]EMR-Group, Geological Institute, RWTH Aachen University, Aachen, 52062, Germany
[2]Institute of Geosciences, Kiel University, Kiel, 24118, Germany
[3]Department of Natural History Sciences, Faculty of Science, Hokkaido University, Sapporo, 060-0810, Japan
[4]High-Precision Mass Spectrometry and Environment Change Laboratory (HISPEC), Department of Geosciences, National Taiwan University, Taipei, 10617, Taiwan ROC
[5]Research Center for Future Earth, National Taiwan University, Taipei, LC6L73, Taiwan ROC
[6]Global Change Research Center, National Taiwan University, Taipei, 10617, Taiwan, ROC
[7]Department of Ocean Systems, Royal Netherlands Institute for Sea Research (NIOZ), and Utrecht University, 1790 AB Den Burg, The Netherlands

Correspondence to: Maike Leupold (maike.leupold@emr.rwth-aachen.de)

Abstract. The dominant modes of climate variability on interannual timescales in the tropical Indian Ocean are the El Niño Southern Oscillation (ENSO) and the Indian Ocean Dipole. El Niño events have occurred more frequently during recent decades and it has been suggested that an asymmetric ENSO teleconnection (warming during El Niño events is stronger than cooling during La Niña events) caused the pronounced warming of the western Indian Ocean. In this study, we test this hypothesis using coral Sr/Ca records from the central Indian Ocean (Chagos Archipelago) to reconstruct past sea surface temperatures (SST) in time windows from the mid-Little Ice Age (1675-1716) to the present. Three sub-fossil massive *Porites* corals were dated to the 17-18th century (one sample) and 19-20th century (two samples), and were compared with a published, modern coral Sr/Ca record from the same site. All corals were sub-sampled at a monthly resolution for Sr/Ca measurements, which were measured using a simultaneous ICP-OES. Wavelet coherence analysis shows that interannual variability in the four coral records is driven by ENSO, suggesting that the ENSO-SST teleconnection in the central Indian Ocean was stationary since the 17th century. To determine the symmetry of El Niño/La Niña events, we compiled composite records of positive and negative ENSO-driven SST anomaly events. We find similar magnitudes of warm and cold anomalies indicating a symmetric ENSO response in the tropical Indian Ocean. This suggests that ENSO is not the main driver of central Indian Ocean warming.

1 Introduction

As the impacts of global climate change increase, paleoclimate research is more important than ever. The Indian Ocean is of major relevance to global ocean warming as the western Indian Ocean has been warming faster than any other ocean basin

during the last century and is the largest contributor to the current rise of global mean sea surface temperatures (Roxy et al., 2014).

Tropical corals can be used to reconstruct past changes of environmental parameters, such as sea surface temperatures (SST), by measuring Sr/Ca. They can help to determine changes in past climate variability. Most coral paleoclimatological studies covering periods before 1900 conducted in the tropical Indian Ocean predominantly focused on $\delta^{18}O$ measurements (e.g. Abram et al., 2015; Charles et al., 2003; Cole et al., 2000; Nakamura, et al., 2011; Pfeiffer et al., 2004). Several studies included Sr/Ca measurements for SST reconstructions in the central, tropical Indian Ocean (Pfeiffer et al., 2006, 2009; Storz et al., 2013; Zinke et al., 2016), while others focused on the western or the eastern Indian Ocean (Abram et al., 2003; Abram et al., 2020; Hennekam et al., 2018; Watanabe et al., 2019) and/or on corals sampled at only bimonthly (Zinke et al., 2004; Zinke et al., 2008) or annual resolution (Zinke et al., 2014; Zinke et al, 2015). The lack of monthly resolved coral Sr/Ca data from the central, tropical Indian Ocean limits our understanding of its response to transregional climate phenomena, as these are phase-locked to the seasonal cycle and vary with season.

Past El Niño Southern Oscillation (ENSO) variability on seasonal and interannual timescales has been reconstructed using corals from different settings in the Pacific Ocean (e.g. Cobb et al., 2003, 2013; Freund et al., 2019; Grothe et al., 2019; Lawman et al., 2020; Li et al., 2011), where ENSO is centered. Strong events associated with ENSO occur more frequently since the early 1980s relative to past centuries (Baker et al., 2008; Freund et al., 2019; Sagar et al., 2016). An intensification of future extreme El Niño/La Niña events under global warming is supported by paleoclimate studies using corals from the central tropical Pacific Ocean (Grothe et al., 2019). Although ENSO is centered in the tropical Pacific Ocean, ocean-atmosphere parameters of the Indian Ocean are influenced by ENSO, which was shown in coral-based SST reconstructions of ENSO variability (e.g. Abram et al., 2008; Marshall and McCulloch, 2001; Storz and Gischler, 2011; Zinke et al., 2004). Strong El Niño/La Niña events influence the tropical Indian Ocean demonstrating a stationary SST-ENSO teleconnection between the Pacific and Indian Ocean (Charles et al., 1997; Cole et al., 2000; Pfeiffer and Dullo, 2006; Wieners et al., 2017). El Niño events cause a basin-wide warming of the Indian Ocean in boreal winter (December-February), while La Niña events cause cooling (Roxy et al., 2014). However, it has been suggested that El Niño events have a stronger influence on the Indian Ocean SSTs than La Niña events, i.e. the warming during El Niño events is larger than the cooling during La Niña events (Roxy et al., 2014). In their study, Roxy et al. (2014) suggest that this asymmetric ENSO teleconnection is one reason for the overall warming of the western Indian Ocean. The positive skewness of SST in the ENSO region of the tropical Pacific is due to ENSO asymmetry, i.e. it reflects the fact that El Niño events are often stronger than La Niña events (Burgers and Stevenson, 1999; An and Jin, 2004). At teleconnected sites, such as the tropical Indian Ocean, the response to El Niño and La Niña may be asymmetric as well, as suggested by Roxy et al. (2014). However, teleconnected sites may also show a symmetric response to El Niño and La Niña events (e.g. Brönniman et al., 2007).

As the impact of ENSO on SSTs in the central Indian Ocean is recorded in coral Sr/Ca records (e.g. Pfeiffer et al., 2006), we test the hypothesis of an asymmetric ENSO teleconnection as a driver of Indian Ocean warming. We use coral Sr/Ca records from three sub-fossil massive *Porites* corals covering periods of the Little Ice Age (1675-1716, 1836-1867), and the mid-19th

to early 20th century (1870-1909) as well as a 20th century coral core (1880-1995) from the central Indian Ocean (Chagos Archipelago) to reconstruct past SST variability. In this study, the concept of 'asymmetric' and 'symmetric' ENSO teleconnection refers to the magnitudes of warming/cooling during El Niño/La Niña events., i.e. we examine whether Indian Ocean warming during El Niño events is stronger than cooling during La Niña events. First, we determine whether ENSO variability is recorded in all coral Sr/Ca records from Chagos, then we identify past warm and cold events in each coral record and compile composites of warm and cold events. We then compare the magnitudes of positive and negative ENSO-driven SST anomalies in the Chagos coral Sr/Ca records and discuss whether or not they provide evidence for an asymmetric ENSO teleconnection in the tropical Indian Ocean.

2 Regional setting

2.1 Location

The Chagos Archipelago is located in the tropical Indian Ocean (70-74° E; 4-8° S), about 500 km south of the Maldives. It consists of several atolls with islands, submerged and drowned atolls, and other submerged banks with the Great Chagos Bank being the world's largest atoll (Fig. 1). The Great Chagos Bank covers an area of 18.000 km^2 with eight islands totaling 445 ha of land. Its lagoon has a maximum depth of 84 m and a mean depth of 50 m. Due to its large size and submerged islands, water exchange with the open ocean is substantial. The Salomon atoll is located about 135 km towards the northeast of Eagle Island. Its atoll area is about 38 km^2 and has an enclosed lagoon and an island area > 300 ha. The greatest depth of its lagoon is 33 m, with mean depth of 25 m.

2.2 Climate

Chagos is situated in a region characterized by monsoon climate (Sheppard et al., 2012). The austral summer is the wet season, with the Northeast monsoon lasting from October to February (Pfeiffer et al., 2004). Light to moderate north-west trades blow. During the rest of the year, strong winds from the southeast dominate from April to October (Sheppard et al., 1999).

Chagos lies at the eastern rim of the so-called Seychelles-Chagos thermocline ridge (SCTR). Along that region, a shallow thermocline causes open-ocean upwelling of cold waters. Upwelling along this region was first identified by McCreary et al. (1993) and is forced by both negative and positive wind stress curl (Hermes and Reason, 2009; McCreary et al., 1993). Compared to other upwelling regions of the Indian Ocean, the sea surface temperatures of the SCTR are relatively high. They vary between 28.5°C and 30°C in austral summer. The SCTR is believed to play a major role in the climate variability of this region on different timescales (e.g. Hermes and Reason, 2008; Vialard et al., 2009) with very strong air-sea interaction due to open ocean upwelling combined with relatively warm SST (Sheppard et al., 2012).

On interannual timescales, the dominant mode of climate variability in the SCTR is the El Niño Southern Oscillation (ENSO). During El Niño events, the West Pacific warm pool is displaced towards the East resulting in cooler than normal SST in the Western Pacific and a basin-wide warming of the Indian Ocean (Izumo et al., 2014; Sheppard et al., 2013). Figure 2 compares

the positive SST anomalies during El Niño with the negative SST anomalies during La Niña events in the Indian and Pacific Ocean between 1982 and 2016, as inferred from 'Reynolds' OI v2 SST data (Reynolds et al., 2002; averaged over December-February). Even if not as strong as in the Pacific Ocean, an ENSO response in the tropical Indian Ocean can be observed (Fig. 2). Coupled ocean-atmosphere instabilities centered in the tropical Indian Ocean result in Indian Ocean Dipole (IOD) events (Saji et al., 1999; Sheppard et al., 2013; Webster et al., 1999). A negative (positive) IOD event is defined by warmer (cooler) than normal SST in the eastern part of the Indian Ocean and cooler (warmer) than normal SST in the western Indian Ocean. Several studies showed that the IOD is an inherent mode of variability of the Indian Ocean (e.g. Ashok et al., 2003; Krishnaswamy et al., 2015; Saji et al., 1999; Webster et al., 1999). However, IOD events tend to co-occur with El Niño/La Niña events (e.g. Luo et al, 2010; Saji and Yamagata, 2003). The instrumental record of past IOD events does not go back further than 1960 (Saji and Yamagata, 2003). Coral-based reconstructions of past IOD events over the past millennium suggest a recent intensification of the IOD (Abram et al., 2008; Abram et al., 2020). The corals show few strong IOD events (i.e. 2019, 1997/98, 1961, 1877/78 and 1675), of which only three events (2019, 1961, 1675) occur independently of ENSO. However, neither in 1675 nor in 1961 a positive anomaly can be found in our coral SST records. We therefore decided to treat positive SST anomaly events found in our records as El Niño events even if they could be a result of IOD events independent from or overlapping with El Niño/La Niña events.

2.3 Instrumental data

High-resolution SST data of the AVHRR satellite product (Casey et al., 2010) reveal different mean SST and seasonality at Chagos depending on the reef setting (Leupold et al., 2019; Fig. 3; 28.1±0.9°C for the open ocean reef and 28.5±0.6°C for the lagoon setting averaged over the period 1997-2012). At the open ocean reefs, where upwelling occurs, seasonal minima in SST are colder than in the lagoon, whereas maximum temperatures are not significantly different (t-value = 0.27; p-value = 0.79). Averaged over the entire area of the Chagos (70-74° E; 4-8° S), SST is similar to SST measured in the lagoon. Long-term monthly SST anomalies (i.e. mean seasonal cycle removed) reveal that extreme SST events, such as El Niño in 1997/98 or La Niña in 2010/11, have the same magnitude in both lagoon and open ocean settings (Fig. 3b). Both anomaly records are not significantly different (t-value = 0.34; p-value = 0.37). This suggests that the magnitudes of ENSO signals at Chagos should be recorded in all coral records analyzed in this study.

2.4 ENSO indices

The instrumental record of past El Niño/La Niña events is restricted to the late 19th and early 20th century. Reconstructions of past ENSO events differ depending on the statistics and/or proxies used (see e.g. Wilson et al., 2010 and Brönnimann et al., 2007 for a discussion). We therefore use different ENSO indices for comparison with our coral data presented briefly in the following. The annual El Niño Index *Niño3.4* (Wilson et al., 2010), which was reconstructed using data from the central Pacific (corals), the TexMex region of the USA (tree rings) and other regions in the Tropics (corals and an ice core), was used as a time series of past El Niño/La Niña events that extends beyond the instrumental period, until 1607. In this study, the El Niño

Index *Niño3.4* by Wilson et al. (2010) is further referred to as 'Wilson Niño Index'. We use the Wilson Niño Index for comparison with our coral SST records performing Wavelet Coherence Analysis in the time domain (see section 4.4). Data on the occurrence and magnitude of historical El Niño/La Niña events have been taken from Brönnimann et al. (2007), who combined several reconstructed ENSO indices, climate field reconstructions and early instrumental data, and evaluated them for consistency. Their reconstruction period extends back to 1500 (La Niña events) and 1511 (El Niño events), respectively. We also include the classical ENSO reconstruction of Quinn (1993), which extends back until 1500. As this reconstruction is based on historical observations of various aspects of ENSO, it should be relatively independent from statistical biases. Both records (Quinn, 1993; Brönnimann et al., 2007) cover all our coral time windows, including our 17th century coral record. By including the original list of Quinn (1993), alongside with the updated list of Brönnimann et al. (2007), we aim to evaluate the sensitivity of our analysis to different ENSO reconstructions. We use both indices by Quinn (1993) and Brönnimann et al. (2007) for identifying past warm and cold events in each coral record and we use these events to compile composites (see section 4.5).

3 Methods and materials

3.1 Coral collection and preparation

For this study, three sub-fossil coral samples were collected in February 2010, from boulder beaches and derelict buildings of former settlements at Chagos (Fig. S1). The sub-fossil corals record 41 years of a period from the mid-Little Ice Age (1675-1716), which coincides with the Maunder Minimum, a period of reduced sunspots observations (Eddy, 1976), 31 years of the late Little Ice Age (1836-1867) and 39 years of the mid-19th to early 20th century (1870-1909). Samples E3 (1870-1909) and E5 (1675-1716) were taken from Eagle Island (S 6°11.39'; E 71°19.58'), an island on the western rim of the Great Chagos Bank (Fig. 1). Sample B8 (1836-1867) was taken from the lagoon-facing site of Boddam Island (S 5°21.56'; E 72°12.34') in the southwestern part of the Salomon atoll. The samples were cross-sectioned into 0.7-1.0 cm thick slabs and X-rayed with a Faxitron X-ray model 43885 operated at 50 keV for 1-2 minutes and used together with a Konica-Minolta Regius ∑ RC 300 reader. From the slabs of each sub-fossil coral, powder samples were drilled at 1 mm increments using a micro-milling machine (type PROXXON FF 500 CNC). This depth resolution can be translated to monthly temporal resolution with average growth rates being 12 mm/yr. The subsampling paths were always set along the optimal growth axis that was determined based on x-ray images (Fig. S2).

Core GIM, a modern coral core, was included in the coral composite of the SCTR (Pfeiffer et al., 2017). This composite comprises cores from the Seychelles and Chagos. Additionally, the core top (1950-1995) of the GIM core has been calibrated with SST (Pfeiffer et al., 2009). Core GIM, was drilled underwater in 1995 in the lagoon of Peros Banhos, located in the northwest of Chagos, from a living coral colony. The monthly coral Sr/Ca record of GIM extends from 1880-1995. Analytical procedures have been described in Pfeiffer et al. (2009). In this study, we use this core to estimate the magnitude of modern El Niño/La Niña events.

3.2 Coral Sr/Ca analysis

Sr/Ca ratio measurements were performed at Kiel University using a Spectro Ciros CCD SOP inductively coupled plasma optical emission spectrometer (ICP-OES) following a combination of techniques described by Schrag (1999) and de Villiers et al. (2002). Elemental emission signals were simultaneously collected and subsequently drift corrected by sample-standard bracketing every six samples. Between 0.13 and 0.65 mg of coral powder was dissolved in 1.00 mL 0.2 M HNO_3. Prior to analysis, the solution was diluted with 0.2 M HNO3 to a final concentration of approximately 8ppm Calcium. Strontium and Calcium intensity lines used are 421 nm and 317 nm, respectively. The intensities of Strontium and Calcium were converted into Sr/Ca ratios in mmol/mol. Before and after each measurement sequence (n = 448 measurements), a stack of 8 different reference materials, including the international reference materials, JCp-1 and JCt-1 (Hathorne et al., 2013), were measured and used for calibration. For drift-correction, an in-house coral reference standard (Mayotte coral) was used. Average analytical precision of Sr/Ca determinations is 0.08% relative standard deviation (RSD) or 0.008 mmol/mol (n = 1973), translating into a temperature of around 0.1°C. The reproducibility of Sr/Ca ratios from multiple measurements both on the same day and on consecutive days is 0.08% RSD (n = 238; 1SD), translating into a temperature uncertainty of around 0.1°C.

3.3 Chronology

Each sub-fossil coral sample was dated by U-Th in 2016. U-Th isotopic measurements were performed with an MC-ICPMS (Thermo Electron Neptune) in the High-Precision Mass Spectrometry and Environment Change Laboratory (HISPEC) of the Department of Geosciences, National Taiwan University (NTU), following techniques described in Shen et al. (2012). U-Th isotopic compositions and concentrations are listed in Table 1.

Sample E5 covers the period from 1675 to 1716, herein further referred to as E5 (1675-1716). Sample B8 covers the period from 1836 to 1867, E3 from 1870 to 1909, both referred to as B8 (1836-1867) and E3 (1870-1909), respectively. The uncertainties of the age models are approximately ±1.9 years (E5), ±2.2 years (B8) and ±2.4 years (E3). All age models were verified by a second, independently measured U-Th age of each sample, measured in 2017 in the HISPEC laboratory of the Department of Geosciences, NTU, following techniques described in Shen et al. (2012). These age determinations are consistent with our Sr/Ca chronologies.

The chronology of the samples was developed based on seasonal cycles of coral Sr/Ca and by analyzing the density bands visible on x-ray images (Fig. S2). We assigned the highest Sr/Ca value to the SST minimum of each year and interpolated linearly between these anchor points to obtain a time series with equidistant time steps.

3.4 Diagenesis screening

A combination of X-ray diffraction (XRD), optical and scanning electron microscopy (SEM) was used to investigate potential diagenetic alteration in the sub-fossil coral samples from Chagos that may affect the Sr/Ca values (Figs. S3, S4, and S5).

Representative samples for thin-section, scanning electron microscopy (SEM) and X-ray diffraction (XRD) analysis were selected from all corals based on the X-ray images. The 2-D-XRD system Bruker D8 ADVANCE GADDS at the Rheinisch-Westfaelische Technische Hochschule (RWTH) Aachen was used for non-destructive XRD point-measurements directly on thin-section blocks with a calcite detection limit of ~ 0.2 % (Smodej et al., 2015). For each coral sample diagenetic modifications were analyzed using one thin-section, one sample for SEM, one 2D-XRD measurement and one powder-XRD measurement.

3.5 Statistics

All coral Sr/Ca records were centered, i.e. normalized with respect to their mean values (Pfeiffer et al., 2009) and translated into SST using a temperature dependence of -0.06 mmol/mol per 1°C for *Porites* corals at Chagos (Leupold et al., 2019; Pfeiffer et al., 2009).

Wavelet coherence plots between the coral Sr/Ca records and the Wilson Niño Index were generated using the *MATLAB* (version R2019b) software toolboxes by Groth and Ghil (2015) to assess whether the interannual variability recorded in the corals is related to ENSO.

Composites of El Niño and La Niña events were generated by calculating the mean of positive and negative anomaly events taken from centered monthly coral SST anomaly records. By centering the coral records to their mean and focusing on interannual variability, we eliminate the largest uncertainty of single-core Sr/Ca records, as shown by Sayani et al. (2019).

T-tests were conducted using the free web application *T-Test Calculator* (GraphPad QuickCalcs, 2019; https://www.graphpad.com/quickcalcs/ttest1/, last access: 09 April, 2019). T-tests were used to determine if the mean values of two data sets, e.g. mean annual cycles in chapter 4.3 or mean anomalies of coral composites in chapter 4.5, are significantly different from each other.

As the significance of the monthly mean anomalies calculated for the composite records depends on the numbers of events, standard errors (SE) for monthly mean anomaly values were used and calculated as follows:

$$SE = \frac{\text{standard deviation } (\sigma)}{\sqrt{\text{Number of events (n)}}}, \quad (1)$$

4 Results and Interpretation

4.1 Diagenesis

Only trace amounts of diagenetic phases were detected in the sub-fossil coral samples, which show a good to excellent preservation according to the criteria defined in Cobb et al. (2013). Isolated scalenohedral calcite cement crystals were observed in the thin-section of E5 (1675-1716) (Fig. S3 a-d). However, XRD results and SEM analysis confirm that the calcite abundance is below the detection limit of XRD (0.2%) in this sample (Fig. S3 e-f). B8 (1836-1867) shows trace amounts of patchily distributed, thin aragonite cements (Fig. S4). E3 (1870-1909) is devoid of diagenetic phases (Fig. S5), but in some

areas of the thin-section dissolution of centers of calcification can be seen (Fig. S5 c-d). Slight dissolution and microborings are also visible under SEM (Fig. S5 f). However, microborings are always open and therefore will not influence the geochemistry. In summary, diagenesis screening revealed that the coral samples are suitable for conducting geochemical analysis and diagenetic modifications to the Sr/Ca records should be neglectable.

4.2 Sr/Ca measurements

Table 2 gives an overview of the Sr/Ca ratios of each sub-fossil coral core and statistical key figures of the records. The values are shown in Figure 4.

4.2.1 17-18th century

A total of 472 subsamples from E5 (1675-1716) was measured for Sr/Ca. The average Sr/Ca value is 8.96 ± 0.07 mmol/mol (n = 472). The maximum range of all Sr/Ca values over the 41-year sample span is 0.41 mmol/mol, between a minimum of 8.73 mmol/mol and a maximum of 9.14 mmol/mol.

4.2.2 19-20th century

From B8 (1836-1867), Sr/Ca of 375 subsamples was measured. The average value is 9.02 ± 0.07 mmol/mol (n = 375) over a range of 0.51 mmol/mol. The maximum Sr/Ca value for the 31-year sample span is 9.36 mmol/mol, the minimum Sr/Ca value is 8.85 mmol/mol.

For E3 (1870-1909), Sr/Ca measurements were conducted on 415 subsamples. The average Sr/Ca value is 8.95 ± 0.06 mmol/mol (n = 415) for the 39-year sample span, over a range of 0.38 mmol/mol from a minimum value of 8.79 mmol/mol to a maximum of 9.17 mmol/mol.

4.3 Decadal variability and seasonal cycle

All coral SST records show variability on decadal scale (Fig. 4). Such decadal variability in the Indian Ocean was already described in previous studies (Charles et al., 1997; Cole et al., 2000; Pfeiffer et al., 2006, 2009; Zinke et al., 2008), and the typical periodicity is 9-13 years. Within a decadal cool/warm phase, negative/positive SST anomalies may occur. In particular, high-amplitude, short-term cool events are possible as Chagos lies in a region where open ocean upwelling occurs (see Leupold et al., 2019). To ensure that decadal variability does not influence the composite records (by inflating interannual warm or cool anomalies), decadal variability is removed by detrending the coral records.

The mean annual cycles of all sub-fossil coral SST records are not significantly different as indicated by p-values around 1 in the t-tests (Table 3, Fig. 4). The seasonal amplitudes in coral SST (°C) are slightly higher in E5 (1675-1716) (1.99°C) compared to B8 (1836-1867) (1.81°C) and E3 (1870-1909) (1.71°C). A shift of mean maximum temperatures from February (E5 and B8) to April (E3) can be observed (Fig. 4). Seasonal amplitudes explain 26-32% of the coral-SST variance (see supplementary material and Fig. S6).

4.4 ENSO signals in coral SST records

The modern and the sub-fossil coral SST records were compared with the annually resolved Wilson Niño Index that extends back until 1607 (Wilson et al., 2010). All coral records show positive and negative SST anomalies, which occur in years where El Niño/La Niña events have been reported (Fig. 5). To analyze a possible correlation between the coral SST records and ENSO, Wavelet Coherence (WTC) was conducted on all coral records and the Wilson Niño Index (Wilson et al., 2010). Wavelet Coherence (WTC) plots were generated to find regions in time-frequency space where the Wilson Niño Index and the Chagos coral SST records co-vary, even if they do not have high power in those regions (Fig. 6).

All WTC plots of the Wilson Niño Index and coral SST records reveal time-localized areas of strong coherence occurring in periods that correspond to the characteristic ENSO cycles of two to eight years. The WTC plots for the Wilson Niño Index and the 19-20th century coral records show several regions where both time series co-vary. In contrast, the WTC plot of the Wilson Niño Index and the 17-18th century coral SST record shows only one region of co-variation at the beginning of the 18th century. The plots show that there is an approximate lag of 9 months to one year between the 17-18th century coral SST record and the Wilson Niño Index (Fig. 6a), and an approximate 1-3 year lag between B8 (1836-1867) and E3 (1870-1909) and the Wilson Niño Index, respectively, (Figs. 6b & c). However, the lags between the coral SST and the index time series are in the range of the age model uncertainties of the sub-fossil corals, and do not represent real time lags. For a further comparison of the coral SST records' and the Wilson Niño Index' frequencies, singular spectrum analysis and power spectra of non-detrended and detrended time series were computed (see supplementary material).

All coral records show anomaly events that can be explained with El Niño/La Niña events listed in Quinn (1993) or Brönnimann et al. (2007) (Tables 4-6). Our results show that, compared to the 17-18th century, more El Niño/La Niña events per period are recorded in coral records of the central Indian Ocean in recent periods. According to the AVHRR satellite data and coral records, an El Niño event occurs on average every 4 years between 1981 and 2017 (AVHRR) or every 5 years between 1965 and 1995 (coral record), respectively (Tables 4-6). This is supported by the events listed in Quinn (1993), and reflects a change in ENSO frequency in the tropical Pacific. Overall, predominantly strong El Niño events are recorded by the coral records from Chagos, as indicated in the list of events presented in (Brönnimann et al. (2007) (Table 6). The number of events listed in Brönnimann et al. (2007) is comparable to the number of events recorded in the corals, whereas the number of events listed in Quinn (1993) is higher compared to the events recorded in the corals. The same holds for the negative SST anomaly events (La Niña and non-La Niña events): the number of La Niña events listed in Brönnimann et al. (2007) is similar to the number of negative anomaly events recorded in the coral records. Furthermore, based on the AVHRR satellite data and the coral records, negative anomaly events occurred every 2.6 years (AVHRR) and every 6 years in the coral record or every 5 years in Brönnimann et al. (2007) between 1965 and 1995, respectively. During the 17-18th century, negative SST anomalies occurred every 6.8 years (coral record) or 10.3 years (Brönnimann et al., 2007) (Tables 4-6).

4.5 ENSO composites

Composites of monthly coral SST anomalies were produced for El Niño/La Niña events to assess their magnitudes. Each composite was produced using coral records of several individual El Niño/La Niña events. An overview of the events used for generating each composite can be found in Table 4 and Table 5. An overview of all events found in the coral Sr/Ca records and of El Niño/La Niña events of the corresponding time periods listed in Quinn (1993) and Brönnimann et al. (2007) is given in Table 6. Positive SST anomalies in the coral records were interpreted as El Niño events when the year of occurrence was listed as one El Niño event in Quinn (1993) and Brönnimann et al. (2007) within the error of each coral age model and when the anomaly exceeds 1.5 standard deviations of the mean of each coral record (Fig. S7). In addition to the strong La Niña events listed in Brönnimann et al. (2007), we added negative SST anomalies occurring in years after the El Niños to the composite.

The composite record for El Niño events comprises 35 events, and 31 events are included in the La Niña composite (Table 4). To investigate changes in the magnitude of ENSO anomalies over time, composites for the time periods 17-18th century and 19-20th century, respectively, were generated. For the 17-18th century, six events (five events) were used for the El Niño (La Niña) composite. The composite for the 19-20th century includes events from the sub-fossil corals and the GIM record. For the 19-20th century, 29 events (26 events) were used for the El Niño (La Niña) composite. The 19-20th century composites, in turn, were split into three sub-periods: 1830-1929 (18 El Niño events, 16 La Niña events), 1930-1964 (five El Niño events, five La Niña events; Table 5) and 1965-1995 (six El Niño events, five La Niña events). These sub-periods were chosen because ENSO activity was reduced between 1930 and 1965 compared to before 1930 and after 1965 (e.g. Cole et al., 1993).

Observations indicate that some upwelling events in the central Indian Ocean are not forced by large-scale ENSO or IOD variability but associated with cyclonic wind stress curls in the southern tropical Indian Ocean (Dilmahamod et al., 2016; Hermes and Reason, 2009). Such an upwelling event occurred in August 2002 and was found in both the coral and satellite SST records at Chagos (see Leupold et al., 2019).

To investigate the potential effect of such negative anomaly events on the La Niña composites, the 19-20th century composites were split up into composites of La Niña events and other negative anomaly events, which are not related to La Niña. La Niña and negative anomalies other than La Niña events were selected based on the months they occurred in, i.e. November-May (La Niña), June-September (Non-La Niña). As such events are also observed recently, we compared modern (1981-2018) satellite SST composites for El Niño events (nine events), La Niña events (10 events) and negative anomalies other than La Niña events (four events) with our coral SST composites. We used the AVHRR satellite SST (Casey et al., 2010) averaged over entire Chagos (4-8° S; 70-74° W).

4.5.1 Positive anomalies in coral and satellite SST composites

The coral SST composites of positive SST anomalies reveal that corals of the central Indian Ocean record higher anomalies during El Niño events compared to the satellite composites (Fig. 7), which may reflect the greater sensitivity of the corals to

reef-scale temperatures (Leupold et al., 2019) or the different time periods covered by these records (only two El Niño events in the AVHRR record overlap with the coral data). The coral composite of the 17-18th century shows higher anomalies than the coral composites of the 19-20th century (Fig. 7). All positive SST anomalies identified as El Niño events in the coral records show on average a maximum value of 1.5 ± 0.1°C (n = 35; Fig. 7). The average maximum temperature anomaly value of El Niño events during the 17-18th century were 2.2 ± 0.2°C (n = 6), higher than and significantly different ($p << 0.01$) from the average maximum El Niño temperature anomaly during the 19-20th century (1.3 ± 0.1°C; n = 29). The average maximum temperature of El Niño events picked from the AVHRR satellite SST (covering the period from 1981 to 2018) of 0.8 ± 0.1°C (n = 9) is also lower than and significantly different ($p << 0.01$) from average maximum El Niño temperature anomaly in the 19-20th century. This suggests a greater impact of El Niño events on Indian Ocean SST during the 17-18th century compared to the 19-20th century and during the last decades.

4.5.2 Negative anomalies in coral and satellite SST composites

No statistically significant differences were found between negative anomalies in coral SST in the central Indian Ocean during the 17-18th century and the 19-20th century and between La Niña and non-La Niña events (Fig. 8).

All negative SST anomalies identified as La Niña and non-La Niña events in the coral records show a minimum temperature anomaly of -1.6 ± 0.1°C (n = 31) on average (Fig. 8). On average, the minimum temperature anomaly is -1.6 ± 0.1°C (n = 22) for all La Niña events and -1.5 ± 0.4°C (n = 9) for non-La Niña events during the 19-20th century of the coral SST records ($p = 0.75$). La Niña events in the coral records are slightly more negative than non-La Niña events, but not statistically different from non-La Niña events ($p = 0.60$). The same is observed in the AVHRR satellite SST anomaly composites, where average La Niña minimum temperature anomalies are -0.8 ± 0.1°C (n = 10) and non-La Niña anomalies are -0.6 ± 0.1°C (n = 4; $p = 0.17$).

The average minimum temperature anomalies of La Niña and non-La Niña events during the 17-18th century were slightly less extreme (-1.5 ± 0.3°C; n = 5), but not significantly different ($p = 0.73$) from the average minimum temperature anomalies of the 19-20th century (-1.6 ± 0.2°C; n = 26).

4.5.3 Interannual SST anomalies during the 19th and 20th century

Dividing the 19-20th century into three sub-periods (1830-1929; 1930-1964; 1965-1995) and compiling SST anomaly composites allows us to assess changes in the magnitude of ENSO-driven warm and cold anomalies over time (Fig. 9). The El Niño composites do not show any systematic changes during the 19-20th century in the Indian Ocean. For the period between 1830 and 1929, the average maximum temperature anomaly is 1.4 ± 0.1°C (n = 18), while between 1930 and 1964 the average maximum temperature anomaly of 1.2 ± 0.1°C (n = 5) is slightly less extreme than the previous period, but not significantly different ($p = 0.5$). For the last period of the 20th century, 1965 to 1995, the average maximum temperature anomaly is again to 1.4 ± 0.1°C (n = 6; Fig. 9).

The magnitude of cooling during La Niña and non-La Niña events tend to reduce from 1830-1929 to 1965-1995 (Fig. 9). For the period between 1830 and 1929, the average minimum temperature anomaly is -1.9 ± 0.2°C (n = 16). Between 1930 and 1964 the average minimum temperature anomaly increases by 0.58°C to -1.3 ± 0.1°C (n = 5), and for 1965 to 1995, the average minimum temperature anomaly is -1.1 ± 0.1°C (n = 5). However, for both El Niño and La Niña events, the differences between the means of the first period (1830-1929) and the last period (1965-1995) are not statistically significant ($p = 0.93$; $p = 0.07$, respectively).

5 Discussion

It has been shown that ENSO influenced SST variability of the Indian Ocean during the 19th and 20th century (Charles et al., 1997; Cole et al., 2000) and that there was a stationary ENSO-SST teleconnection, in the sense that El Niño warms the Indian Ocean and La Niña cools it (Pfeiffer and Dullo, 2006). Our results show that all coral records, covering periods of the 17-18th and 19-20th century, show interannual variability that is coherent with the Wilson Niño Index. We therefore can say that the ENSO-SST teleconnection in the central Indian Ocean was stationary since 1675.

In this study, we aim to take the analysis of the ENSO-SST teleconnection one step further: we have compiled the data in composites to estimate and compare the magnitude of ENSO-induced warming and cooling in the central Indian Ocean. This allows us to assess the symmetry/asymmetry of the ENSO teleconnection. Overall, the magnitudes of El Niño and La Niña events recorded in the Chagos coral records during the past century are comparable (Fig. 9). This suggests the ENSO teleconnection in the tropical Indian Ocean was close to symmetric. Only in times of cooler mean climates (during the 17-18th century), the corals seem to indicate higher amplitude ENSO-induced warm anomalies in the tropical Indian Ocean, although these differences are not statistically significant. Hence, our results do not support the notion that an asymmetric ENSO teleconnection with strong warming during El Niño years drives the recent warming of the tropical Indian Ocean as suggested by Roxy et al. (2014). The modern coral records from the central Indian Ocean all show a steady warming during the 20th century, and this warming continuous in the time interval of reduced ENSO activity between 1930 and 1965 (e.g. Charles et al., 1997; Pfeiffer and Dullo, 2006; Abram et al., 2016). This suggests that neither the magnitude, nor the frequency of past El Niño events explains the centennial-scale warming of the Indian Ocean.

El Niño/La Niña events recorded in our coral records and listed in Table 4 and 5 can be found as predominantly “very strong” or “strong” events listed in Quinn (1993) and Brönnimann et al. (2007) (Table 6). As it can be seen in Table 6, all positive anomaly events recorded in our coral records can be explained with one event listed in either Quinn (1993) or Brönnimann et al. (2007). Not every event listed in Quinn (1993) and Brönnimann et al. (2007) is recorded in the coral records from the central Indian Ocean. Especially the number of events in Quinn (1993) is higher compared to the events recorded in the coral records. However, the number of events listed in Brönnimann et al. (2007) is similar to the number of events recorded in the coral records (Table 6), again suggesting that predominantly strong events in the Pacific Ocean (as Brönnimann et al. (2007) only listed strong events) are recorded in the corals from the central Indian Ocean. This in turn implies, that our results are not dependent on the ENSO index used as a basis to identify events, as most reconstructions consistently record strong events.

Our results showing that El Niño events resulted in stronger SST anomalies in the central Indian Ocean corals in the 17-18th century, i.e. during a cooler mean climate, are consistent with Pfeiffer et al., (2017), who found larger amplitudes of ENSO-induced warm anomalies in the tropical Indian Ocean in the late 19th century, when mean SSTs in the tropical Indian Ocean were cooler. It is also consistent with Zinke et al. (2004) who found highest $\delta^{18}O$ amplitude variations in the interannual ENSO band between 1645–1715 in a coral from Ifaty, Madagascar. Comparing both periods, the La Niña and non-La Niña cold events show no significant changes suggesting a stable negative SST anomaly pattern in the Indian Ocean. We are not sure why this is the case. However, the tropical Indian Ocean is the warmest tropical Ocean, and recent instrumental data suggests that, as the Indian Ocean continues to warm, the temperature variability reduces particularly in the warm season, while SSTs in the cold season show strongest warming (e.g. Leupold et al., 2019; Roxy et al., 2014) and largest spatial variability (Leupold et al, 2019).

The coral records from Chagos also record upwelling events in boreal summer, which are independent of ENSO, poorly represented in satellite data of SST (see Leupold et al., 2019), and which may result in the failure of the Indian monsoon. Such an upwelling event occurred for example in 2002 and lead to a drought over the Indian subcontinent (Jayakumar and Gnanaseelan, 2012; Krishnan et al., 2006). At present, little is known about the frequency or magnitudes of these events in past decades or centuries. Coral proxy data from Chagos thus allow us to better understand these non-La Niña upwelling events.

In contrast to the stationary teleconnection between ENSO and SST in the central Indian Ocean, the ENSO-precipitation teleconnection was shown to be non-stationary (Timm et al., 2005). The impact of ENSO on rainfall in the central Indian Ocean depends on mean SSTs, and these surpassed a critical threshold for atmospheric convection in the mid-1970s, strengthening the El Niño signal in rainfall. However, our study does not indicate an increase in the magnitude of El Niño-related SST anomalies following this shift compared to earlier time periods of strong ENSO activity.

In summary, this study confirms that the ENSO-SST teleconnection between the Pacific and Indian Ocean is stationary over the 19th/20th century and back to 1675. We have shown that it is possible to reconstruct interannual SST variations in the tropical Indian Ocean. This is important because so far there exist no reliable high-resolution SST reconstructions in the Indian Ocean covering the periods we studied. SST reconstruction studies of the Pacific Ocean also show ENSO and decadal-scale variability covering the periods from 1998 back to 1886 (Cobb et al., 2001) and 928-961, 1149-1220, 1317-1464 and 1635-1703 (Cobb et al., 2003). Cobb et al. (2003) spliced three overlapping coral records of the 14-15th century and five coral records of the 17-18th century together. We have shown that this approach would be applicable in the tropical Indian Ocean using sub-fossil corals from boulder beaches and historical buildings, and if a more complete record of millennial-scale coral reconstructions from the tropical Pacific and the Indian Ocean becomes available, it will be possible to assess the ENSO teleconnection based on an analysis of the coral records from both oceans. This is important because recent studies have shown that the tropical Indian Ocean plays a pivotal role in 20th century global temperature rise (Funk et al., 2008; Roxy et al., 2014; Pfeiffer et al., 2017).

6 Conclusions

We have shown that the ENSO-SST relationship in the central Indian Ocean was stationary since the 17th century. All four coral records showed interannual variability coherent with ENSO variability, but variations in the intensity of El Niño and La Niña-induced SST anomalies in the central Indian Ocean. El Niño events cause average positive anomalies of 2.2 ± 0.2°C (n = 6) during the 17-18th century and 1.3 ± 0.1°C (n = 29) during the 19-20th century, while La Niña events cause average negative anomalies of -1.5 ± 0.3°C (n = 5) during the 17-18th century and -1.6 ± 0.2°C (n = 26) during the 19-20th century in the central Indian Ocean. However, not all cooling events are related to La Niña events, but also to processes internal to the Indian Ocean causing negative anomalies of -1.5 ± 0.4°C (n = 7) during the 19-20th century. The magnitudes of El Niño and La Niña events during the last century are comparable, indicating a symmetric ENSO teleconnection. An asymmetric ENSO teleconnection being the cause for the overall warming of the central, tropical Indian Ocean appears therefore unlikely. However, we suggest compiling composite records of negative and positive SST anomaly events from additional sub-fossil Indian Ocean corals to further explore the ENSO-SST teleconnection, and how it varies in cooler or warmer climatic intervals.

Author contribution: M.L. conceived the study, wrote the paper and produced all figures. M.P., L.R., T.K.W. and D.G.-S. helped with analyzing and interpreting the data. L.R. assessed the preservation of the coral samples. T.K.W., C.-C.S. and G.-J.B. helped dating the samples and with the development of the age models. M.P. acquired the funding for this project, contributed feedback and helped refine the writing.

Competing interests: The authors declare that they have no competing interests.

Data and materials availability: All methods needed to evaluate the conclusions in the paper are present in the paper and/or the supplementary material. The data plotted in all figures will be available to the public over the Paleoclimatology Branch of NOAA's National Center for Environmental Information (NCEI) (http://www.ncdc.noaa.gov/data-access/paleoclimatology-data) after the completion of the dissertation of M. Leupold.

Acknowledgments: We thank Karen Bremer for laboratory assistance and the Deutsche Forschungsgemeinschaft (DFG) for funding the projects PF 676/2-1 and PF 676/3-1. Coral U-Th dating was supported by grants from the Science Vanguard Research Program of the Ministry of Science and Technology, Taiwan, ROC (108-2119-M-002-012), the Higher Education Sprout Project of the Ministry of Education, Taiwan, ROC (108L901001), and National Taiwan University (109L8926).

References

Abram, N. J., Gagan, M. K., McCulloch, M. T., Chappell, J., and Hantoro, W. S.: Coral reef death during the 1997 Indian Ocean Dipole linked to Indonesian wildfires, Science, 301(5635), 952-955, https://doi.org/10.1126/science.1083841, 2003.

Abram, N. J., Gagan, M. K., Cole, J. E., Hantoro, W. S., and Mudelsee, M.: Recent intensification of tropical climate variability in the Indian Ocean, Nat. Geosci., 1(12), 849, https://doi.org/10.1038/ngeo357, 2008.

Abram, N. J., Dixon, B. C., Rosevear, M. G., Plunkett, B., Gagan, M. K., Hantoro, W. S., and Phipps, S. J.: Optimized coral reconstructions of the Indian Ocean Dipole: An assessment of location and length considerations, Paleoceanogr. Paleocl., 30(10), 1391-1405, https://doi.org/10.1002/2015pa002810, 2015.

Abram, N. J., McGregor, H. V., Tierney, J. E., Evans, M. N., McKay, N. P., Kaufman, D. S., ... and Steig, E. J.: Early onset of industrial-era warming across the oceans and continents, Nature, 536(7617), 411, https://doi.org/10.1038/nature19082, 2016.

Abram, N. J., Wright, N. M., Ellis, B., Dixon, B. C., Wurtzel, J. B., England, M. H., … and Heslop, D.: Coupling of Indo-Pacific climate variability over the last millennium, Nature, 579, 385–392, https://doi.org/10.1038/s41586-020-2084-4, 2020.

An, S. I., and Jin, F. F.: Nonlinearity and asymmetry of ENSO, J. Climate, 17(12), 2399-2412, https://doi.org/10.1175/1520-0442(2004)017<2399:NAAOE>2.0.CO;2, 2004.

Ashok, K., Guan, Z., and Yamagata, T.: A look at the relationship between the ENSO and the Indian Ocean dipole, J. Meteorol. Soc. Jpn. Ser. II, 81(1), 41-56, https://doi.org/10.2151/jmsj.81.41, 2003.

Baker, A. C., Glynn, P. W., and Riegl, B.: Climate change and coral reef bleaching: An ecological assessment of long-term impacts, recovery trends and future outlook, Estuar. Coast. Shelf. S., 80(4), 435-471, https://doi.org/10.1016/j.ecss.2008.09.003, 2008.

Brönnimann, S., Xoplaki, E., Casty, C., Pauling, A., and Luterbacher, J.: ENSO influence on Europe during the last centuries, Clim. Dynam., 28(2-3), 181-197, https://doi.org/10.1007/s00382-006-0175-z, 2007.

Burgers, G., and Stephenson, D. B.: The "normality" of El Niño, Geophys. Res. Lett., 26(8), 1027-1030, https://doi.org/10.1029/1999GL900161, 1999.

Casey, K. S., Brandon, T. B., Cornillon, P. and Evans, R.: The Past, Present and Future of the AVHRR Pathfinder SST Program, in: Oceanography from Space, edited by: Barale, V., Gower, J. F. R., and Alberotanza, L., Springer, Dordrecht, NL, 273-287, https://doi.org/10.1007/978-90-481-8681-5_16, 2010.

Charles, C. D., Hunter, D. E., and Fairbanks, R. G.: Interaction between the ENSO and the Asian monsoon in a coral record of tropical climate, Science, 277(5328), 925-928, https://doi.org/10.1126/science.277.5328.925, 1997.

Charles, C. D., Cobb, K. M., Moore, M. D., and Fairbanks, R. G.: Monsoon-tropical ocean interaction in a network of coral records spanning the 20th century, Mar. Geol., 201. https://doi.org/10.1016/S0025-3227(03)00217-2, 2003.

Cobb, K. M., Charles, C. D., and Hunter, D. E.: A central tropical Pacific coral demonstrates Pacific, Indian, and Atlantic decadal climate connections, Geophys. Res. Lett., 28(11), 2209-2212, https://doi.org/10.1029/2001gl012919, 2001.

Cobb, K. M., Charles, C. D., Cheng, H., and Edwards, R. L.: El Niño/Southern Oscillation and tropical Pacific climate during the last millennium, Nature, 424(6946), 271, https://doi.org/10.1038/nature01779, 2003.

Cobb, K. M., Westphal, N., Sayani, H. R., Watson, J. T., Di Lorenzo, E., Cheng, H., ... and Charles, C. D.: Highly variable El Niño–Southern Oscillation throughout the Holocene, Science, 339(6115), 67-70, https://doi.org/10.1126/science.1228246, 2013.

Cole, J. E., Fairbanks, R. G., and Shen, G. T.: Recent variability in the Southern Oscillation: Isotopic results from a Tarawa Atoll coral, Science, 260(5115), 1790-1793, https://doi.org/10.1126/science.260.5115.1790, 1993.

Cole, J. E., Dunbar, R. B., McClanahan, T. R., and Muthiga, N. A.: Tropical Pacific forcing of decadal SST variability in the western Indian Ocean over the past two centuries, Science, 287(5453), 617-619, https://doi.org/10.1126/science.287.5453.617, 2000.

de Villiers, S., Greaves, M. and Elderfield, H.: An intensity ratio calibration method for the accurate determination of Mg/Ca and Sr/Ca of marine carbonates by ICP-AES, Geochem. Geophy. Geosy., 3(1), 1001, https://doi.org/10.1029/2001gc000169, 2002.

Dilmahamod, A. F., Hermes, J. C., and Reason, C. J. C.: Chlorophyll-a variability in the Seychelles–Chagos Thermocline Ridge: Analysis of a coupled biophysical model, J. Marine Syst., 154, 220-232, https://doi.org/10.1016/j.jmarsys.2015.10.011, 2016.

Eddy, J.A.: The Maunder Minimum, Science, 192(4245), 1189-1202, https://doi.org/10.1126/science.192.4245.1189, 1976.

Freund, M. B., Henley, B. J., Karoly, D. J., McGregor, H. V., Abram, N. J., and Dommenget, D.: Higher frequency of Central Pacific El Niño events in recent decades relative to past centuries, Nat. Geosci., 12, 450–455, https://doi.org/10.1038/s41561-019-0353-3, 2019.

Funk, C., Dettinger, M. D., Michaelsen, J. C., Verdin, J. P., Brown, M. E., Barlow, M., and Hoell, A.: Warming of the Indian Ocean threatens eastern and southern African food security but could be mitigated by agricultural development, P. Natl. Acad. Sci USA, 105(32), 11081-11086, https://doi.org/10.1073/pnas.0708196105, 2008.

GraphPad QuickCalcs: T-Test Calculator, Retrieved from https://www.graphpad.com/quickcalcs/ttest1/, last access: 09 April, 2019.

Groth, A., and Ghil, M.: Monte Carlo Singular Spectrum Analysis (SSA) revisited: Detecting oscillator clusters in multivariate datasets, J. Climate, 28, 7873-7893, https://doi.org/10.1175/JCLI-D-15-0100.1, 2015.

Grothe, P. R., Cobb, K. M., Liguori, G., Di Lorenzo, E., Capotondi, A., Lu, … and Toth, L. T.: Enhanced El Niño–Southern Oscillation variability in recent decades. Geophys. Res. Lett., 46, https://doi.org/10.1029/2019GL083906, 2019.

Hammer, Ø., Harper, D. A. T., and Ryan, P. D.: Paleontological statistics software: package for education and data analysis, Palaeontol. Electron., (4), 2001.

Hathorne, E. C., Gagnon, A., Felis, T., Adkins, J., Asami, R., Boer, W., ... and Demenocal, P.: Interlaboratory study for coral Sr/Ca and other element/Ca ratio measurements. Geochem. Geophy. Geosy., 14(9), 3730-3750, https://doi.org/10.1002/ggge.20230, 2013.

Hennekam, R., Zinke, J., van Sebille, E., ten Have, M., Brummer, G.-J. A., & Reichart, G.-J.: Cocos (Keeling) corals reveal 200 Years of multidecadal modulation of southeast Indian Ocean hydrology by Indonesian throughflow, Paleoceanogr. Paleocl., 33, 48– 60. https://doi.org/10.1002/2017PA003181, 2018.

Hermes, J. C., and Reason, C. J. C.: Annual cycle of the South Indian Ocean (Seychelles-Chagos) thermocline ridge in a regional ocean model, J. Geophys. Res.-Oceans, 113(C4), https://doi.org/10.1029/2007jc004363, 2008.

Hermes, J. C., and Reason, C. J. C.: The sensitivity of the Seychelles–Chagos thermocline ridge to large-scale wind anomalies, ICES J. Mar. Sci., 66(7), 1455-1466, 2009.

Hiess, J., Condon, D. J., McLean, N., and Noble, S. R.: 238U/235U systematics in terrestrial uranium-bearing minerals, Science, 335(6076), 1610-1614, https://doi.org/10.1093/icesjms/fsp074, 2012.

Huang, B., Thorne, P. W., Banzon, V. F., Boyer, T., Chepurin, G., Lawrimore, J. H., ... and Zhang, H. M.: Extended reconstructed sea surface temperature, version 5 (ERSSTv5): upgrades, validations, and intercomparisons, J. Climate, 30(20), 8179-8205, https://doi.org/10.1175/jcli-d-16-0836.1, 2017.

Izumo, T., Lengaigne, M., Vialard, J., Luo, J. J., Yamagata, T., and Madec, G.: Influence of Indian Ocean Dipole and Pacific recharge on following year's El Niño: interdecadal robustness, Clim. Dynam., 42(1-2), 291-310, https://doi.org/10.1007/s00382-012-1628-1, 2014.

Jayakumar, A., and Gnanaseelan, C.: Anomalous intraseasonal events in the thermocline ridge region of Southern Tropical Indian Ocean and their regional impacts, J. Geophys. Res.-Oceans, 117(C3), https://doi.org/10.1029/2011jc007357, 2012.

Krishnan, R., Ramesh, K. V., Samala, B. K., Meyers, G., Slingo, J. M., and Fennessy, M. J.: Indian Ocean-monsoon coupled interactions and impending monsoon droughts, Geophys. Res. Lett., 33(8), https://doi.org/10.1029/2006gl025811, 2006.

Krishnaswamy, J., Vaidyanathan, S., Rajagopalan, B., Bonell, M., Sankaran, M., Bhalla, R. S., and Badiger, S.: Non-stationary and non-linear influence of ENSO and Indian Ocean Dipole on the variability of Indian monsoon rainfall and extreme rain events, Clim. Dynam., 45(1-2), 175-184, https://doi.org/10.1007/s00382-014-2288-0, 2015.

Lawman, A. E., Quinn, T. M., Partin,J. W., Thirumalai, K., Taylor, F., … and Shen, C.-C.: A century of reduced ENSO variability during the Medieval Climate Anomaly, Paleoceanogr. Paleocl., 35, https://doi.org/10.1029/2019PA003742, 2020.

Leupold, M., Pfeiffer, M., Garbe-Schönberg, D., and Sheppard, C.: Reef-scale-dependent response of massive Porites corals from the central Indian Ocean to prolonged thermal stress–evidence from coral Sr/Ca measurements, Geochem. Geophy. Geosy., 20(3). https://doi.org/10.1029/2018GC007796, 2019.

Li, J., Xie, S. P., Cook, E. R., Huang, G., D'arrigo, R., Liu, F., ... and Zheng, X. T.: Interdecadal modulation of El Niño amplitude during the past millennium, Nat. clim. change, 1(2), 114-118., https://doi.org/10.1038/nclimate1086, 2011.

Luo, J. J., Zhang, R., Behera, S. K., Masumoto, Y., Jin, F. F., Lukas, R., and Yamagata, T.: Interaction between El Niño and extreme Indian ocean dipole, J. Climate, 23(3), 726-742, https://doi.org/10.1175/2009jcli3104.1, 2010.

Marshall, J. F., & McCulloch, M. T.: Evidence of El Niño and the Indian Ocean Dipole from Sr/Ca derived SSTs for modern corals at Christmas Island, eastern Indian Ocean. Geophys. Res. Lett., 28(18), 3453-3456., 2001.

McCreary, J. P., Kundu, P. K., and Molinari, R. L.: A numerical investigation of dynamics, thermodynamics and mixed-layer processes in the Indian Ocean, Prog. Oceanogr., 31, 181–244, https://doi.org/10.1016/0079-6611(93)90002-u, 1993.

Mudelsee, M.: Ramp function regression: A tool for quantifying climate transitions, Comput. Geosci.-UK, 26(3), 293-307, https://doi.org/10.1016/s0098-3004(99)00141-7, 2000.

Mudelsee, M.: Break function regression: A tool for quantifying trend changes in climate time series, Eur. Phys. J.-Spec. Top., 174(1), 49-63, https://doi.org/10.1140/epjst/e2009-01089-3, 2009.

Nakamura, N., Kayanne, H., Iijima, H., McClanahan, T. R., Behera, S. K., and Yamagata, T.: Footprints of IOD and ENSO in the Kenyan coral record, Geophys. Res. Lett., 38(24), https://doi.org/10.1029/2011gl049877, 2011.

Pfeiffer, M., Dullo, W. C., and Eisenhauer, A.: Variability of the Intertropical Convergence Zone recorded in coral isotopic records from the central Indian Ocean (Chagos Archipelago), Quaternary Res., 61(3), 245-255, https://doi.org/10.1016/j.yqres.2004.02.009, 2004.

Pfeiffer, M., and Dullo, W. C.: Monsoon-induced cooling of the western equatorial Indian Ocean as recorded in coral oxygen isotope records from the Seychelles covering the period of 1840–1994 AD, Quaternary Sci. Rev., 25(9-10), 993-1009, https://doi.org/10.1016/j.quascirev.2005.11.005, 2006.

Pfeiffer, M., Timm, O., Dullo, W. C., and Garbe-Schönberg, D.: Paired coral Sr/Ca and $\delta^{18}O$ records from the Chagos Archipelago: Late twentieth century warming affects rainfall variability in the tropical Indian Ocean, Geology, 34(12), 1069-1072, https://doi.org/10.1130/g23162a.1, 2006.

Pfeiffer, M., Dullo, W. C., Zinke, J., and Garbe-Schönberg, D.: Three monthly coral Sr/Ca records from the Chagos Archipelago covering the period of 1950–1995 AD: reproducibility and implications for quantitative reconstructions of sea surface temperature variations, Int. J. Earth Sci., 98(1), 53-66, https://doi.org/10.1007/s00531-008-0326-z, 2009.

Pfeiffer, M., Zinke, J., Dullo, W. C., Garbe-Schönberg, D., Latif, M., and Weber, M. E.: Indian Ocean corals reveal crucial role of World War II bias for twentieth century warming estimates, Sci. Rep.-UK, 7(1), 14434, https://doi.org/10.1038/s41598-017-14352-6, 2017.

Quinn, W. H.: The large-scale ENSO event, the El Niño and other important regional features, Bull. Inst. fr. études andines, 22(1), 13-34, 1993.

Reynolds, R. W., Rayner, N. A., Smith, T. M., Stokes, D. C., and Wang, W.: An improved in situ and satellite SST analysis for climate, J. Climate, 15(13), 1609-1625, https://doi.org/10.1175/1520-0442(2002)015<1609:aiisas>2.0.co;2, 2002.

Roxy, M., Ritika, K., Terray, P. and Masson, S.: The curious case of Indian Ocean warming, J. Climate 27(22), 8501–8509, https://doi.org/10.1175/JCLI-D-14-00471.1, 2014.

Sagar, N., Hetzinger, S., Pfeiffer, M., Masood Ahmad, S., Dullo, W. C., and Garbe-Schönberg, D.: High-resolution Sr/Ca ratios in a Porites lutea coral from Lakshadweep Archipelago, southeast Arabian Sea: An example from a region experiencing steady rise in the reef temperature, J. Geophys. Res.-Oceans, 121(1), 252-266, https://doi.org/10.1002/2015jc010821, 2016.

Saji, N. H., Goswami, B. N., Vinayachandran, P. N., and Yamagata, T.: A dipole mode in the tropical Indian Ocean, Nature, 401(6751), 360, https://doi.org/10.1038/43854, 1999.

Saji, N. H., and Yamagata, T.: Structure of SST and surface wind variability during Indian Ocean dipole mode events: COADS observations, J. Climate, 16(16), 2735-2751, https://doi.org/10.1175/1520-0442(2003)016<2735:sosasw>2.0.co;2, 2003.

Sayani, H. R., Cobb, K. M., DeLong, K., Hitt, N. T., and Druffel, E. R.: Intercolony $\delta^{18}O$ and Sr/Ca variability among Porites spp. corals at Palmyra Atoll: Toward more robust coral-based estimates of climate, Geochem. Geophy. Geosy., https://doi.org/10.1029/2019gc008420, 2019.

Schrag, D. P.: Rapid analysis of high-precision Sr/Ca ratios in corals and other marine carbonates, Paleoceanography, 14(2), 97-102, https://doi.org/10.1029/1998pa900025, 1999.

Shen, C. C., Cheng, H., Edwards, R. L., Moran, S. B., Edmonds, H. N., Hoff, J. A., and Thomas, R. B.: Measurement of attogram quantities of 231Pa in dissolved and particulate fractions of seawater by isotope dilution thermal ionization mass spectroscopy, Anal. Chem., 75(5), 1075-1079, https://doi.org/10.1021/ac026247r, 2003.

Shen, C. C., Wu, C. C., Cheng, H., Edwards, R. L., Hsieh, Y. T., Gallet, S., ... and Hori, M.: High-precision and high-resolution carbonate 230Th dating by MC-ICP-MS with SEM protocols, Geochim. Cosmochim. Acta, 99, 71-86, https://doi.org/10.1016/j.gca.2012.09.018, 2012.

Sheppard, C. R. C., Seaward, M. R. D., Klaus, R., and Topp, J. M. W.: The Chagos Archipelago: an introduction, in: Ecology of the Chagos Archipelago, edited by: Shepard, C. R. C., and Seaward, M. R. D., Westbury Academic & Scientific Publishing, Otley, UK, 1-20, 1999.

Sheppard, C. R. C., Ateweberhan, M., Bowen, B. W., Carr, P., Chen, C. A., Clubbe, C., ... and Gaither, M. R.: Reefs and islands of the Chagos Archipelago, Indian Ocean: why it is the world's largest no-take marine protected area, Aquat. Conserv., 22(2), 232-261, https://doi.org/10.1002/aqc.1248, 2012.

Sheppard, C. R. C., Bowen, B. W., Chen, A. C., Craig, M. T., Eble, J., Fitzsimmons, N., ... and Koldewey, H.: British Indian Ocean Territory (the Chagos Archipelago): setting, connections and the marine protected area, in: Coral Reefs of the United Kingdom Overseas Territories, Springer, Dordrecht, NL, 223-240, 2013.

Smodej, J., Reuning, L., Wollenberg, U., Zinke, J., Pfeiffer, M., and Kukla, P. A.: Two-dimensional X-ray diffraction as a tool for the rapid, nondestructive detection of low calcite quantities in aragonitic corals, Geochem. Geophy. Geosy., 16(10), 3778-3788, https://doi.org/10.1002/2015gc006009, 2015.

Storz, D., and Gischler, E.: Coral extension rates in the NW Indian Ocean I: reconstruction of 20th century SST variability and monsoon current strength. Geo-Mar. Lett., 31(3), 141-154., https://doi.org/10.1007/s00367-010-0221-z, 2011.

Storz, D., Gischler, E., Fiebig, J., Eisenhauer, A., and Garbe-Schönberg, D.: Evaluation of oxygen isotope and Sr/Ca ratios from a Maldivian scleractinian coral for reconstruction of climate variability in the northwestern Indian Ocean, Palaios, 28(1), 42-55, https://doi.org/10.2110/palo.2012.p12-034r, 2013.

Timm, O., Pfeiffer, M., and Dullo, W. C.: Nonstationary ENSO-precipitation teleconnection over the equatorial Indian Ocean documented in a coral from the Chagos Archipelago, Geophys. Res. Lett., 32(2), https://doi.org/10.1029/2004gl021738, 2005.

Vautard, R., and Ghil, M.: Singular spectrum analysis in nonlinear dynamics, with applications to paleoclimatic time series, Physica D, 35, 395-424, https://doi.org/10.1016/0167-2789(89)90077-8, 1989.

Vialard, J., Duvel, J. P., Mcphaden, M. J., Bouruet-Aubertot, P., Ward, B., Key, E., et al.: Cirene: air–sea interactions in the Seychelles–Chagos thermocline ridge region, B. Am. Meteorol. Soc., 90(1), 45-61, https://doi.org/10.1175/2008bams2499.1, 2009.

Watanabe, T. K., Watanabe, T., Yamazaki, A., Pfeiffer, M., and Claereboudt, M. R.: Oman coral $\delta^{18}O$ seawater record suggests that Western Indian Ocean upwelling uncouples from the Indian Ocean Dipole during the global-warming hiatus, Sci. Rep.-UK, 9(1), 1887, https://doi.org/10.1038/s41598-018-38429-y, 2019.

Webster, P. J., Moore, A. M., Loschnigg, J. P., and Leben, R. R.: Coupled ocean–atmosphere dynamics in the Indian Ocean during 1997–98, Nature, 401(6751), 356, https://doi.org/10.1038/43848, 1999.

Wieners, C. E., Dijkstra, H. A., and de Ruijter, W. P.: The Influence of the Indian Ocean on ENSO Stability and Flavor, J. Climate, 30(7), 2601-2620, https://doi.org/10.1175/jcli-d-16-0516.1, 2017.

Wilson, R., Cook, E., D'Arrigo, R., Riedwyl, N., Evans, M. N., Tudhope, A., and Allan, R.: Reconstructing ENSO: the influence of method, proxy data, climate forcing and teleconnections, J. Quaternary Sci., 25(1), 62-78, https://doi.org/10.1002/jqs.1297, 2010.

Zinke, J., Dullo, W.-C., Heiss, G.A., and Eisenhauer, A.: ENSO and Indian Ocean subtropical dipole variability is recorded in a coral record off southwest Madagascar for the period 1659 to 1995, Earth Planet. Sc. Lett., 228(1-2), 177-194, doi: 10.1016/j.epsl.2004.09.028, https://doi.org/10.1016/j.epsl.2004.09.028, 2004.

Zinke, J., Pfeiffer, M., Timm, O., Dullo, W.-C., Kroon, D., and Thomassin, B. A.: Mayotte coral reveals hydrological changes in the western Indian Ocean between 1881 and 1994, Geophys. Res. Lett., 35(23), https://doi.org/10.1029/2008gl035634, 2008.

Zinke, J., Rountrey, A., Feng, M., Xie, S. P., Dissard, D., Rankenburg, K., Lough, J., and McCulloch, M. T.: Corals record long-term Leeuwin Current variability including Ningaloo Niño/Niña since 1795, Nat. Commun., 5, 3607. https://doi.org/10.1038/ncomms4607, 2014.

Zinke, J., Hoell, A., Lough, J. M., Feng, M., Kuret, A. J., Clarke, H., Ricca, V., Rankenburg, K., and McCulloch, M. T.: Coral record of southeastern Indian Ocean marine heatwaves with intensified Western Pacific temperature gradient, Nat. Commun., 6, 8562. https://doi.org/10.1038/ncomms9562, 2015.

Zinke, J., Reuning, L., Pfeiffer, M., Wassenburg, J. A., Hardman, E., Jhangeer-Khan, R., Davies, G. R., Ng, C. K. C., and Kroon, D.: A sea surface temperature reconstruction for the southern Indian Ocean trade wind belt from corals in Rodrigues Island (19° S, 63° E), Biogeosciences, 13, 5827–5847, https://doi.org/10.5194/bg-13-5827-2016, 2016.

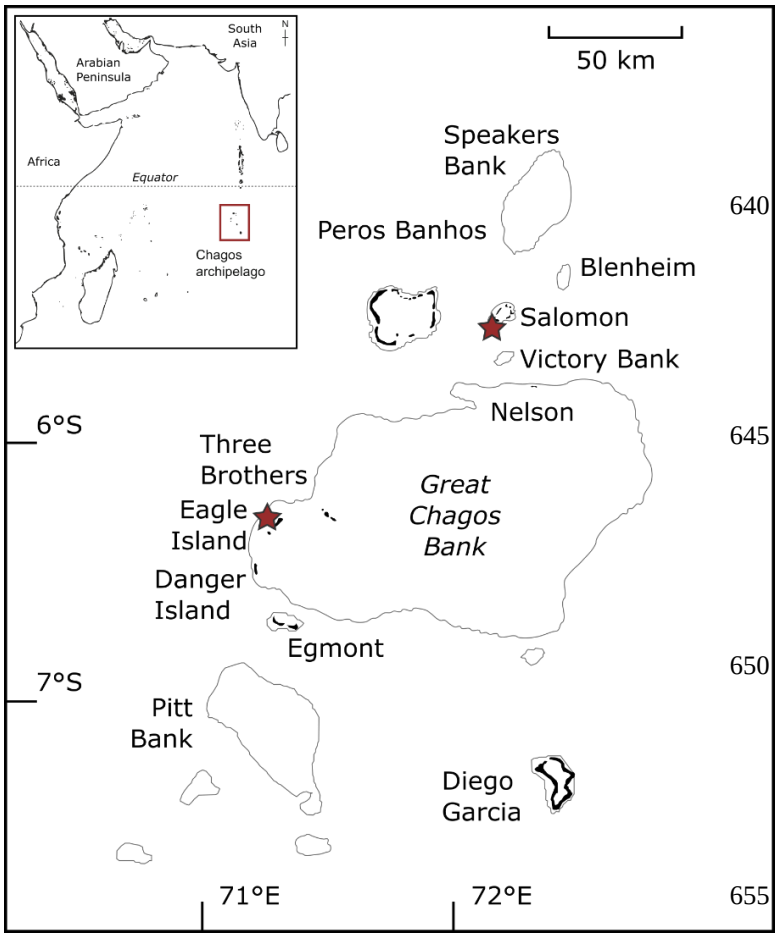

Figure 1: Location of study area and coral sample locations. The Chagos Archipelago is located in the central Indian Ocean, about 550 km south of the Maldives (map upper left). Fossil coral samples were collected on Eagle Island and on Boddam Island (Salomon atoll; red stars).

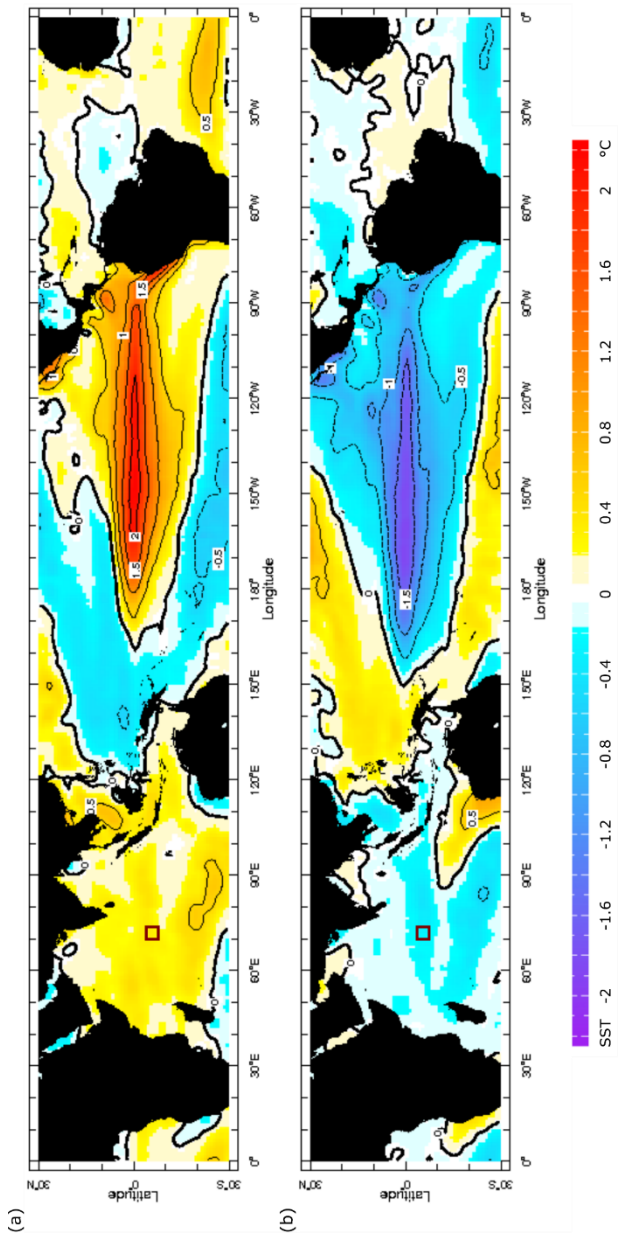

Figure 2: Composite maps of SST anomalies [°C] in the Indian and Pacific Ocean during El Niño/La Niña events. (a) El Niño SST anomalies for the period 1982 to 2016 averaged over December to February. (b) same as in (a), but for La Niña events. SST anomaly maps were computed with NOAA 'Reynolds' OI v2 SST (Reynolds et al., 2002) using the free web application Data Views of the IRI Data Library (https://iridl.ldeo.columbia.edu/). Date accessed: 17 September 2018. Red squares indicate the location of the study area. An overview of all events used for each composite map can be found in Table S1 in the supplementary material.

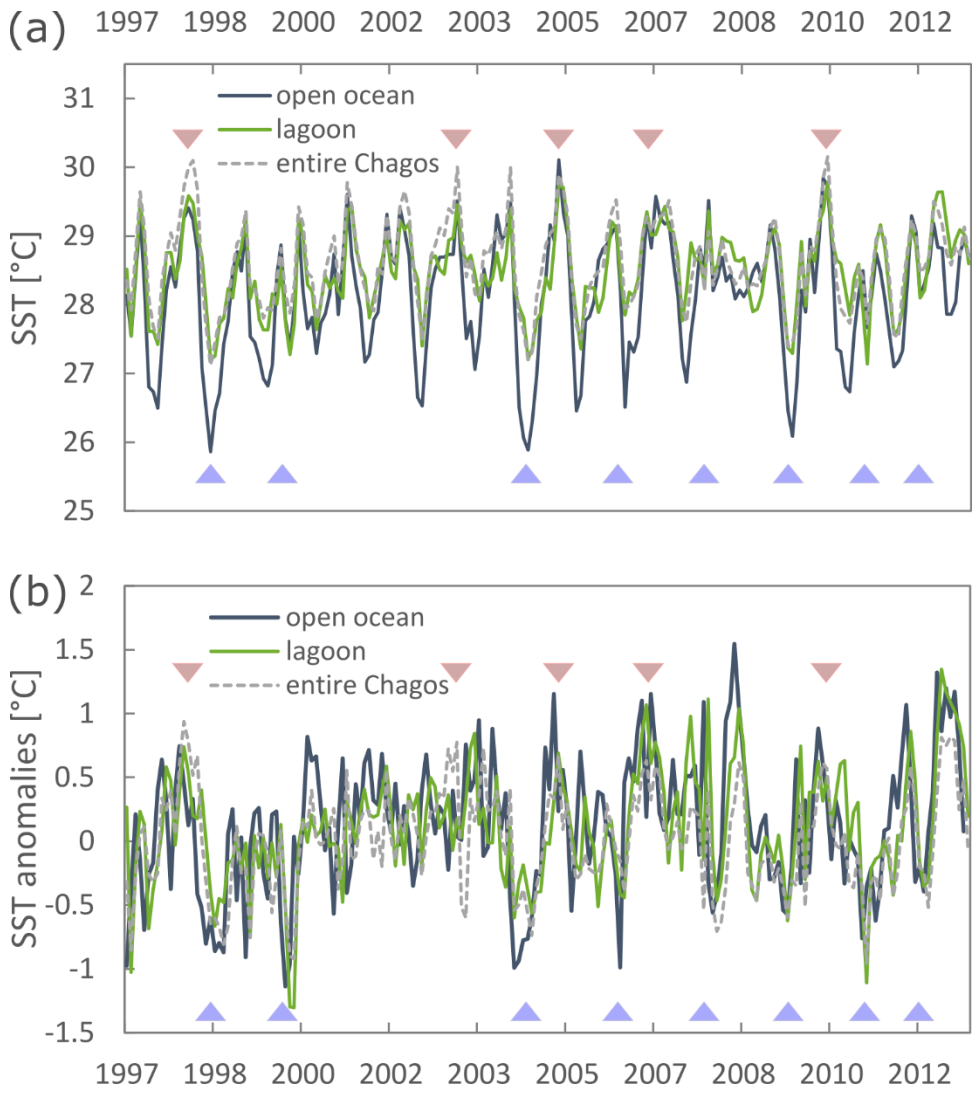

Figure 3: Satellite SST for different settings (lagoon: green; open ocean: blue) and entire Chagos (grey; averaged over 70-74° E; 4-8° S). (a) Monthly satellite SST means and (b) satellite SST anomalies. For the open ocean and lagoon setting we used the high-resolution satellite SST product AVHRR (Casey et al., 2010) and for entire Chagos we used NOAA 'Reynolds' OI v2 SST (Reynolds et al., 2002). Arrows indicate El Niño (red) and La Niña events (blue) based on Brönnimann et al. (2007) and the Oceanic Niño Index ONI (https://www.ggweather.com/enso/oni.htm; Date accessed: 18 October 2018).

coral Sr/Ca-SST [°C]
Year
E5
E3
B8
Month
Aug Oct Dec Feb Apr Jun Aug Oct Dec Feb Apr Jun

Figure 4: Monthly Sr/Ca records (blue lines; converted into coral Sr/Ca-SST in °C) of E5 (1675-1716), B8 (1836-1867) and E3 (1870-1909) with error bars indicating the standard deviation (±2σ) of Sr/Ca ratios from multiple measurements on the same day and on consecutive days and mean annual cycles (black lines and corresponding standard errors highlighted in gray, lower plot).

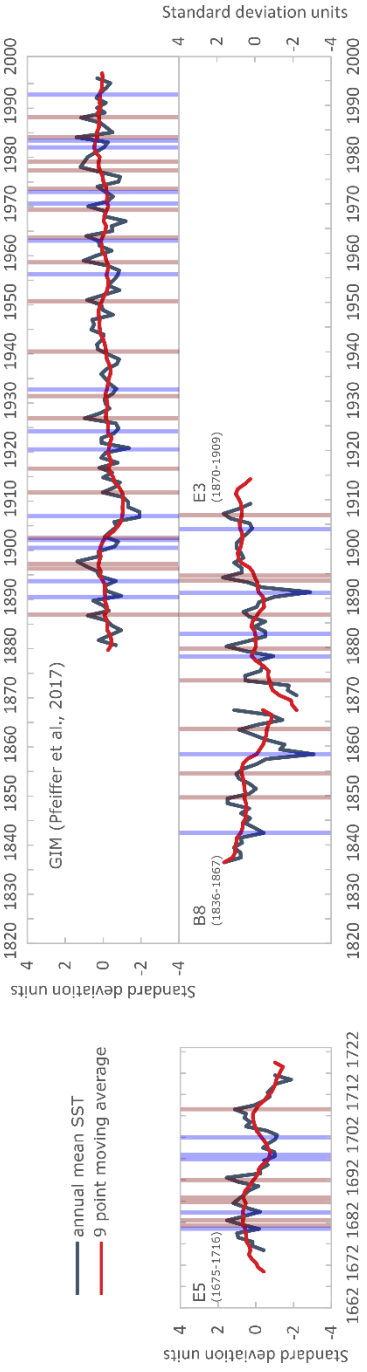

Figure 5: Annual SST anomalies for Chagos corals (this study and GIM from Pfeiffer et al. 2009, 2017) Red- (El Niño) and blue- (La Niña) shaded boxes indicate years used for the composite records (Figs. 7-9). Red thick lines are 9 point moving averages. See text Sect. 4.5 for how El Niño/La Niña events were picked.

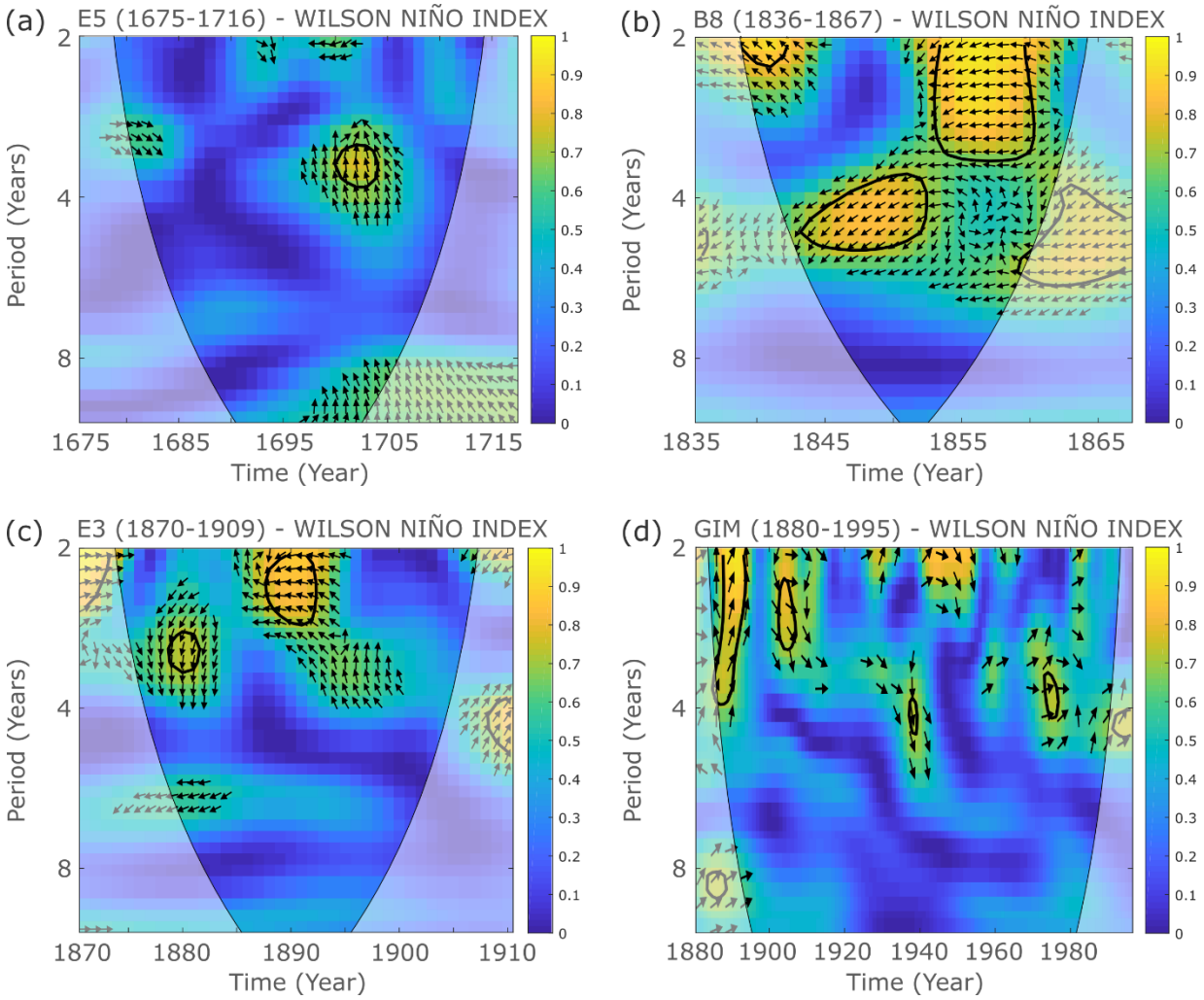

Figure 6: Wavelet coherence analysis plots for the Wilson Niño Index (Wilson et al., 2010) and Chagos coral SST of (a) E5 (1675-1716), (b) B8 (1836-1867), (c) E3 (1870-1909) and (d) GIM (1980-1995).

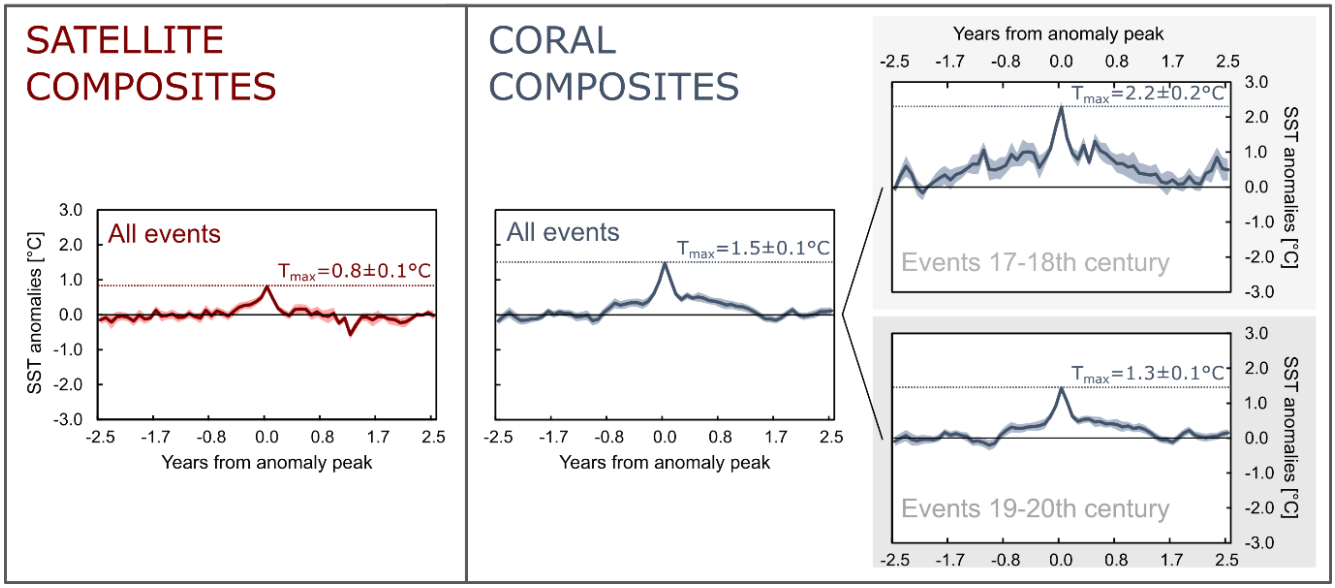

Figure 7: Positive SST anomalies (El Niño) composite records of AVHRR (left; red) and coral SST (right; blue) records. Separate composites of anomaly events during the 17-18th and 19-20th century were generated from the coral SST records. Shaded areas below and above the curves show the standard error for the mean values of the composite records. Table 4 for an overview of the events that were selected for generating the composites.

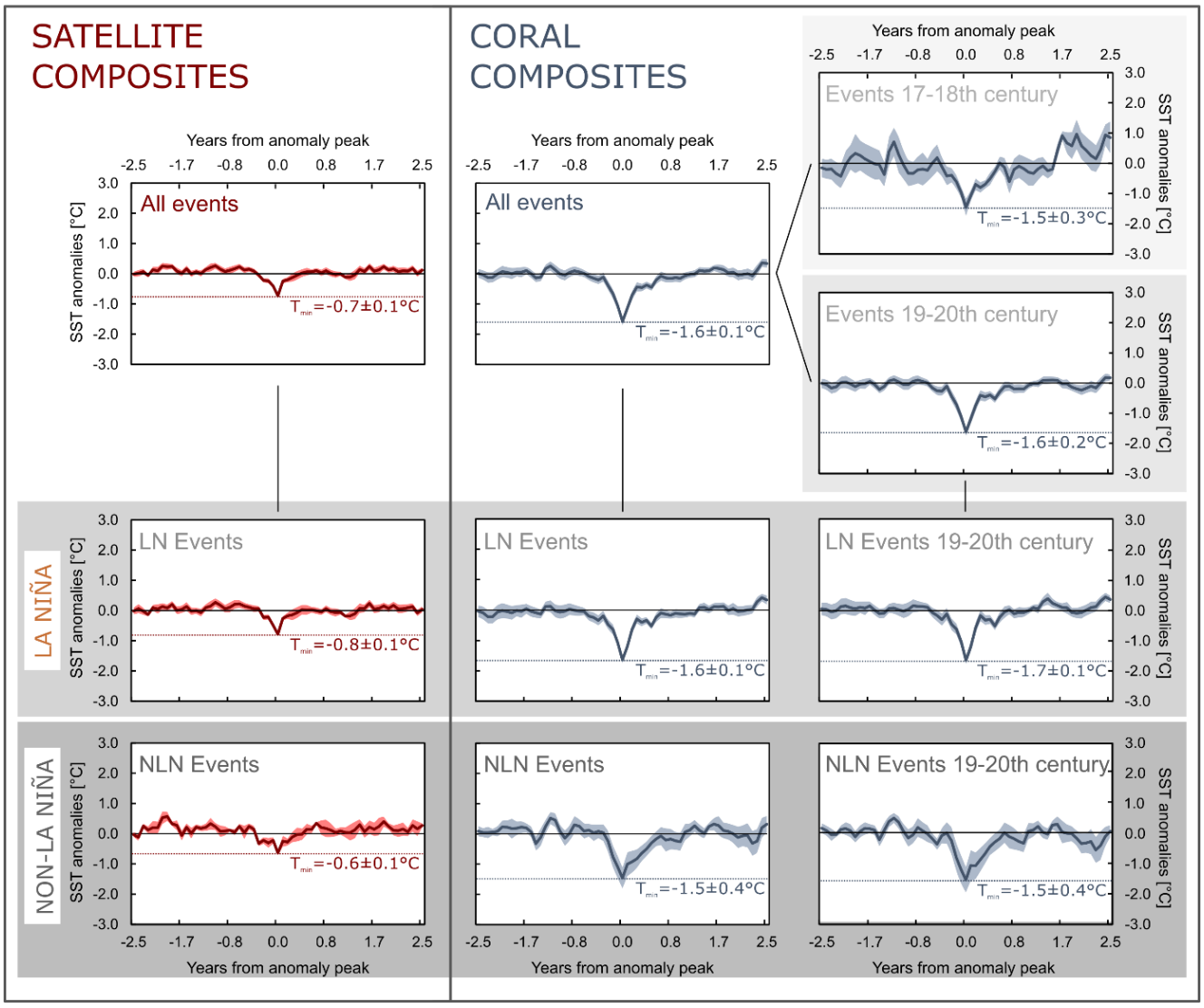

Figure 8: Negative SST anomalies (La Niña and non-La Niña) composite records of AVHRR satellite (left) and coral SST (right) records. Additionally, composites of anomaly events separated by 17-18th and 19-20th century events and by La Niña and non-La Niña events were generated. Shaded areas below and above the curves show the standard error for the mean values of the composite records. See Table 4 for an overview of the events that were selected for generating the composites.

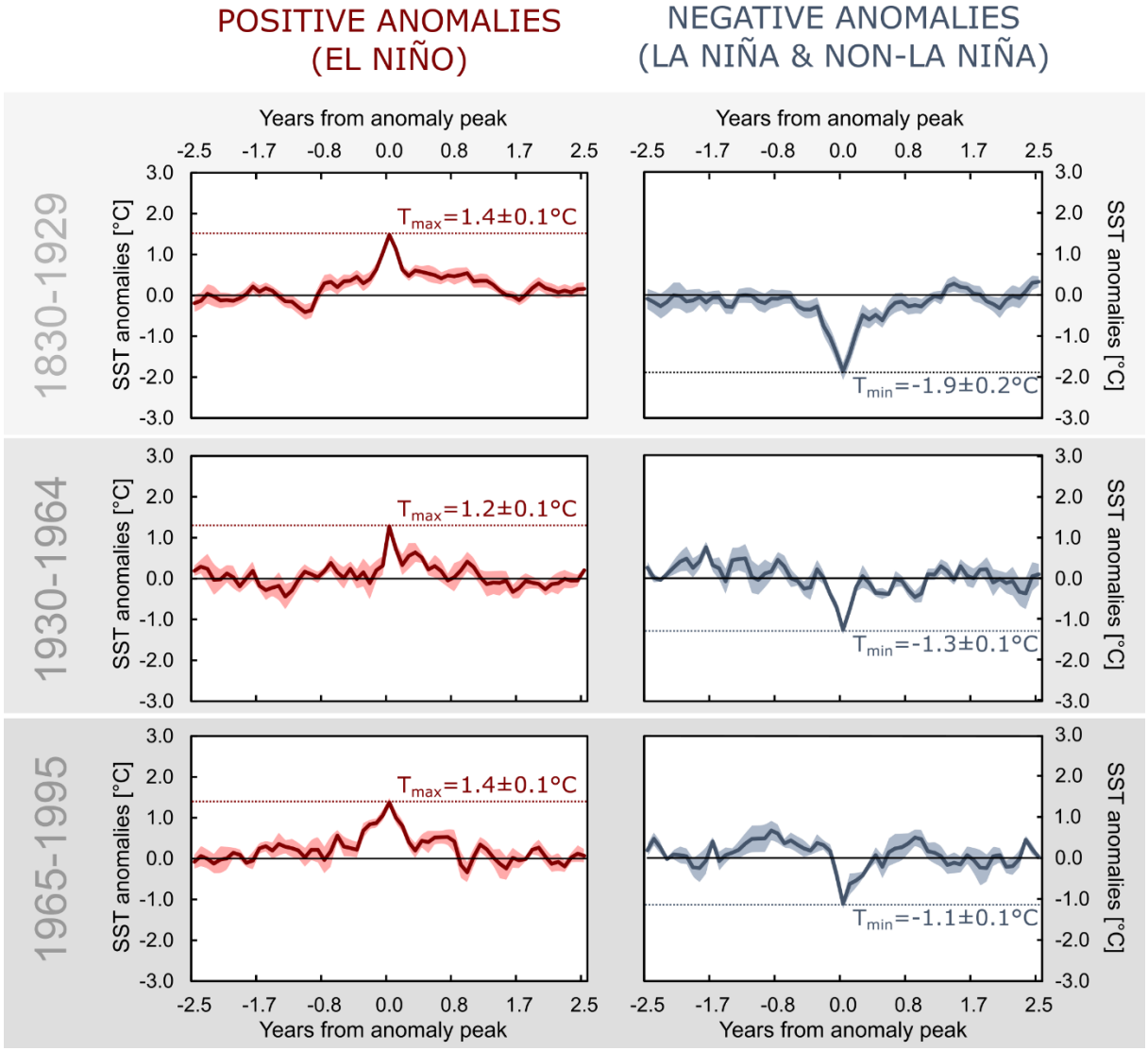

Figure 9: Positive (El Niño; left) and negative SST anomalies (La Niña and non-La Niña; right) composite records of the 19-20th century coral SST records separated by the time intervals 1830-1929 (upper row), 1930-1964 (middle row) and 1965-1995 (lower row). Shaded areas below and above the curves show the standard error for the mean values of the composites records. See Table 5 for an overview of the events that were selected for generating the composites.

Table 1: Overview of Uranium and Thorium isotopic compositions and ^{230}Th ages and corresponding years for fossil coral samples E5 (1675-1716), B8 (1836-1867) and E3 (1870-1909) measured with MC-ICPMS, Thermo Electron Neptune, at NTU. Location of measurement numbers are indicated on x-ray images in Figure S2. Chemistry was performed on March.11th, 2016 and on July 16, 2017 (Shen et al., 2003), and instrumental analysis on MC-ICP-MS (Shen et al., 2012).

Sample ID	Measurement No.	^{238}U (ppb[a])	^{232}Th (ppt)	d^{234}U (measured[a])	[^{230}Th/^{238}U] (activity[c])	[^{230}Th/^{232}Th] (ppm[d])	Age (uncorrected)	Age (corrected[c,e])	d$^{234}U_{initial}$ (corrected[b])	Corresponding year (BP)
E5 (1675-1716)	1st	2265,7 ± 2,3	74,1 ± 3,0	146,4 ± 1,3	0,003250 ± 0,000019	1639 ± 66	309,5 ± 1,9	308,8 ± 1,9	146,6 ± 1,3	1706 ± 1.9
	2nd	2293,9 ± 2,2	16,1 ± 1,3	145,0 ± 1,6	0,003594 ± 0,000018	8458 ± 675	342,8 ± 1,8	342,6 ± 1,8	145,2 ± 1,6	1674 ± 1.8
B8 (1836-1867)	1st	2212,7 ± 2,5	37,1 ± 4,1	144,1 ± 1,5	0,001872 ± 0,000023	1840 ± 203	178,5 ± 2,2	178,1 ± 2,2	144,2 ± 1,5	1838 ± 2.2
	2nd	2386,1 ± 2,1	515,4 ± 1,4	146,2 ± 1,3	0,001650 ± 0,000029	126 ± 2	157,1 ± 2,8	152,1 ± 3,7	146,2 ± 1,3	1865 ± 3.7
E3 (1870-1909)	1st	2551,9 ± 2,5	56,7 ± 3,9	145,4 ± 1,3	0,001194 ± 0,000025	886 ± 64	113,8 ± 2,4	113,3 ± 2,4	145,4 ± 1,3	1903 ± 2.4
	2nd	2694 ± 2,8	643 ± 2	144,7 ± 1,7	0,0015 ± 0,00002	106 ± 1	146 ± 2	141 ± 3,2	145 ± 1,7	1876 ± 3.2

Analytical errors are 2σ of the mean.

[a] $[^{238}U] = [^{235}U] \times 137.818$ (±0.65‰) (Hiess et al., 2012); $\delta^{234}U = ([^{234}U/^{238}U]_{activity} - 1) \times 1000$.

[b] δ^{234}Uinitial corrected was calculated based on ^{230}Th age (T), i.e., $\delta^{234}U_{initial} = \delta^{234}$Umeasured X $e^{\lambda 234*T}$, and *T* is corrected age.

[c] $[^{230}Th/^{238}U]_{activity} = 1 - e^{-\lambda 230T} + (\delta^{234}U_{measured}/1000)[\lambda_{230}/(\lambda_{230} - \lambda_{234})](\lambda - e^{-(\lambda 230 - \lambda 234)T})$, where *T* is the age.

[d] The degree of detrital ^{230}Th contamination is indicated by the $[^{230}Th/^{232}Th]$ atomic ratio instead of the activity ratio.

[e] Age corrections, relative to chemistry date, for samples were calculated using an estimated atomic $^{230}Th/^{232}Th$ ratio of 4 ± 2 ppm.

Those are the values for a material at secular equilibrium, with the crustal $^{232}Th/^{238}U$ value of 3.8. The errors are arbitrarily assumed to be 50%.

Table 2: Statistical overview for raw Sr/Ca data.

Sample	Amount subsamples	Sr/Ca [mmol/mol]						median RSD [%]
		Mean	Median	Std dev	Min	Max	Range	
E5 (1675-1716)	472	8.96	8.96	0.07	8.73	9.14	0.410	0.076
B8 (1836-1867)	375	9.02	9.02	0.07	8.85	9.36	0.506	0.075
E3 (1870-1909)	415	8.95	8.95	0.06	8.79	9.17	0.376	0.074

Table 3: Statistical overview for mean annual cycle data of the coral Sr/Ca-SST [°C] records.

Sample	Max	Min	Amplitude	Mean	SD	P-value of t-test (two-tailed)		
						E5 (1675-1716) vs.	B8 (1836-1867) vs.	E3 (1870-1909) vs.
E5 (1675-1716)	0.70	-1.29	1.99	0.0026	0.5459		0.9979	0.9991
B8 (1836-1867)	0.61	-1.21	1.82	0.0033	0.5450	0.9979		0.9969

E3 (1870-1909)	0.60	-1.11	1.71	0.0024	0.5089	0.9991	0.9969	

***Note*. SD is the standard deviation.**

	Composite		Years with events	Number of events	Records used
Postive SST anomalies	Coral Composites	all events	1679, 1682, 1686, 1687, 1691, 1708, 1849, 1853, 1863, 1873, 1879, 1881, 1886 (2x), 1889, 1894, 1895, 1896, 1897, 1902, 1907, 1911, 1916, 1926, 1932, 1940, 1951, 1958, 1963, 1969, 1973, 1977, 1979, 1983, 1987	35	E5 (1675-1716), B8 (1836-1867), E3 (1870-1909), GIM (1880-1995)
		17-18th century	1679, 1682, 1686, 1687, 1691, 1708	6	E5 (1675-1716)
		19-20th century	1849, 1853, 1863, 1873, 1879, 1881, 1886 (2x), 1889, 1894, 1895, 1896, 1897, 1902, 1907, 1911, 1916, 1926, 1932, 1940, 1951, 1958, 1963, 1969, 1973, 1977, 1979, 1983, 1987	29	B8 (1836-1867), E3 (1870-1909), GIM (1880-1995)
	Satellite Composite	all events	1983, 1987, 1988, 1998, 2003, 2005, 2007, 2015, 2016	9	AVHRR SST (1981-2018)
Negative SST anomalies	Coral Composites	all events	1680, 1684, 1697, 1698, 1702, 1846, 1858, 1860, 1865, 1872, 1883, 1890, 1891, 1893, 1895, 1900, 1902, 1903, 1906, 1920, 1924, 1932, 1947, 1952, 1956, 1964, 1970, 1974, 1982, 1984, 1994	31 (22 LN, 9 NLN)	E5 (1675-1716), B8 (1836-1867), E3 (1870-1909), GIM (1880-1995)
		17-18th century	1680, 1684, 1697, 1698, 1702	5	E5 (1675-1716)
		19-20th century	1846, 1858, 1860, 1865, 1872, 1883, 1890, 1891, 1893, 1895, 1900, 1902, 1903, 1906, 1920, 1924, 1932, 1947, 1952, 1956, 1964, 1970, 1974, 1982, 1984, 1994	26 (19 LN, 7 NLN)	B8 (1836-1867), E3 (1870-1909), GIM (1880-1995)
	Satellite Composite	all events	1984, 1989, 1989, 1992, 1995, 1996, 1998, 2000, 2004, 2008, 2011, 2012, 2014, 2017	14 (10 LN, 4 NLN)	AVHRR SST (1981-2018)

Table 4: Positive (El Niño) and negative (La Niña and non-La Niña) SST anomaly events picked for generating coral and satellite composite records shown in Figure 7 and Figure 8.

19-20th century Coral Composite	Period	Years with events	Number of events	Records used
Postive SST anomalies	1830-1929	1849, 1853, 1863, 1873, 1879, 1981, 1886 (2x), 1889, 1894, 1895, 1896, 1897, 1902, 1907, 1911, 1916, 1926	18	B8 (1836-1867), E3 (1870-1909), GIM (1880-1995)
	1930-1964	1932, 1940, 1951, 1958, 1963	5	GIM (1880-1995)
	1965-1995	1969, 1973, 1977, 1979, 1983, 1987	6	GIM (1880-1995)
Negative SST anomalies	1830-1929	1846, 1858, 1860, 1865, 1872, 1883, 1890, 1891, 1893, 1895, 1900, 1902, 1903, 1906, 1920, 1924	16	B8 (1836-1867), E3 (1870-1909), GIM (1880-1995)
	1930-1964	1932, 1947, 1952, 1956, 1964	5	GIM (1880-1995)
	1965-1995	1970, 1974, 1982, 1984, 1994	5	GIM (1880-1995)

Table 5: 19-20th century (divided into three periods) positive (El Niño) and negative (La Niña and non-La Niña) SST anomaly events picked for generating coral composite records shown in Figure 9.

735

	Positive SST Anomalies						Negative SST Anomalies			
	Events in Records		Published ENSO events				Events in Records		Published ENSO events	
			Quinn (1993)		Brönnimann et al. (2007)				Brönnimann et al. (2007)	
	Years	Numbers of events	Years of very strong (VS), strong (S), medium (M) and weak (W) events	Numbers of events	Years of strong events	Numbers of events	Years	Numbers of events	Years of strong events	Numbers of events
E5 (1675-1716)	1678/79, 1682/83, 1685/86, 1686/87, 1691/92, 1707/08	6	1681 (S), 1684 (M+), 1687-88 (S+), 1692-93 (S), 1696-97 (M+), 1701 (S+), 1707-09 (M/S), 1715-16 (S)	8	1674, 1675, 1677, 1681, 1682, 1691, 1702	7	1680, 1683/84, 1697, 1697/98, 1702	5	1676, 1678, 1698, 1704	4
B8 (1836-1867)	1848/49, 1853/54, 1862/63	3	1837 (M+), 1844-46 (M/S+), 1850 (M), 1852 (M), 1854 (M), 1857-58 (M), 1860 (M), 1862 (M-), 1864 (S), 1866 (M+), 1867-68 (M+)	11	1833, 1846, 1852, 1856, 1869	5	1845/46, 1858, 1860/61, 1864/65	4	1842, 1847, 1863	3
E3 (1870-1909)	1872/73, 1879/80, 1885/86, 1893/94, 1894/95, 1906/07	6	1871 (S+), 1874 (M), 1877-78 (VS), 1880 (M), 1884 (S+), 1887-89 (M+), 1891 (VS), 1897 (M+), 1899-1900 (S), 1902 (M+), 1904-05 (M-), 1907 (M)	12	1869, 1877, 1878, 1889, 1897, 1900, 1903, 1906, 1912	9	1872, 1882/83, 1891, 1895/96, 1903/04	5	1872, 1887, 1890, 1893, 1904, 1910	6
GIM (1880-1995)*	1880/81, 1885/86, 1888/89, 1896/97, 1897, 1902, 1911/12, 1916/17, 1925/26, 1931/32, 1939/40, 1950/51, 1957/58, 1962/63, 1969/70, 1972/73, 1977/78, 1978/79, 1982/83, 1986/87	20	1880 (M), 1884 (S+), 1887-89 (M-/M+), 1891 (VS), 1897 (M+), 1899-90 (S), 1902 (M+), 1904-05 (M-), 1907 (M), 1910 (M+), 1911-12 (S), 1914-15 (M+), 1917 (S), 1923 (M), 1925-26 (VS), 1930-31 (M), 1932 (S), 1939 (M+), 1940-41 (S), 1943 (M+), 1951 (M-), 1953 (M+), 1957-58 (S), 1965 (M+), 1969 (M-), 1972-73 (S), 1976 (M), 1978-79 (W), 1982-83 (VS), 1987 (M), 1991-92 (M), 1994-95 (M-)	32	1878, 1889, 1897, 1900, 1903, 1906, 1912, 1915, 1919, 1926, 1931, 1940, 1941, 1952, 1958, 1966, 1973, 1977, 1983, 1987, 1992	21	1889/90, 1893, 1899/00, 1901/02, 1906, 1919/20, 1924, 1931/32, 1947, 1956, 1951/52, 1964, 1970, 1973/74, 1982, 1983/84, 1993/94	17	1887, 1890, 1893, 1904, 1910, 1917, 1925, 1934, 1943, 1950, 1956, 1968, 1971, 1974, 1976, 1985, 1989	17
AVHRR*	1982/83, 1986/87, 1987/88, 1997/98, 2002/03, 2004/05, 2006/07, 2014/15, 2015/16	9	1982/83 (VS), 1986/87 (M), 1987/88 (S), 1991/92 (S), 1994/95 (M), 1997/98 (VS), 2002/03 (M), 2004/05 (W), 2006/07 (W), 2009/10 (M), 2014/15 (W), 2015/16 (VS)	12	/	/	1984/85, 1989, 1989, 1992, 1995, 1996/97, 1998/99, 1999/00, 2004, 2007/08, 2010/11, 2011/12, 2014, 2016/17	14	1983/84 (W), 1984/85 (W), 1988/89 (S), 1992, 1995/96 (M), 1996/97, 1998/99 (S), 1999/00 (S), 2000/01 (W), 2004, 2005/06 (W), 2007/08 (S), 2008/09 (W), 2010/11 (S), 2011/12 (M), 2014, 2016/17 (W), 2017/18 (W)	18

* Note: Recent events (from 1980 on) were additionally picked using events listed on this website: https://www.ggweather.com/enso/oni.htm (Date accessed: 18 October 2018)

Table 6: Overview of all events found in the coral Sr/Ca records and of El Niño/La Niña events of the corresponding time periods listed in publications. Events in coral records were matched with published events in consideration of age model uncertainties of each coral record.